Article

Phages overcome bacterial immunity via diverse anti-defence proteins

https://doi.org/10.1038/s41586-023-06869-w

Received: 1 May 2023

Accepted: 14 November 2023

Published online: 22 November 2023

Check for updates

Erez Yirmiya[1,5], Azita Leavitt[1,5], Allen Lu[2,3], Adelyn E. Ragucci[2,3], Carmel Avraham[1], Ilya Osterman[1], Jeremy Garb[1], Sadie P. Antine[2,3], Sarah E. Mooney[2,3], Samuel J. Hobbs[2,3], Philip J. Kranzusch[2,3,4], Gil Amitai[1]✉ & Rotem Sorek[1]✉

It was recently shown that bacteria use, apart from CRISPR–Cas and restriction systems, a considerable diversity of phage resistance systems[1–4], but it is largely unknown how phages cope with this multilayered bacterial immunity. Here we analysed groups of closely related *Bacillus* phages that showed differential sensitivity to bacterial defence systems, and discovered four distinct families of anti-defence proteins that inhibit the Gabija, Thoeris and Hachiman systems. We show that these proteins Gad1, Gad2, Tad2 and Had1 efficiently cancel the defensive activity when co-expressed with the respective defence system or introduced into phage genomes. Homologues of these anti-defence proteins are found in hundreds of phages that infect taxonomically diverse bacterial species. We show that the anti-Gabija protein Gad1 blocks the ability of the Gabija defence complex to cleave phage-derived DNA. Our data further reveal that the anti-Thoeris protein Tad2 is a 'sponge' that sequesters the immune signalling molecules produced by Thoeris TIR-domain proteins in response to phage infection. Our results demonstrate that phages encode an arsenal of anti-defence proteins that can disable a variety of bacterial defence mechanisms.

The arms race between bacteria and their viruses has fuelled the evolution of defence systems that protect bacteria from phage infection[1–4]. Phages, in return, developed mechanisms that allow them to overcome bacterial defences[5]. Multiple phages were shown to encode anti-restriction proteins, which inhibit restriction-modification systems by direct binding to the restriction enzyme[6,7] or by masking restriction sites[8]. Phages are also known to encode many CRISPR–Cas inhibitors, which function through a variety of mechanisms including inhibition of CRISPR RNA loading[9], diversion of the CRISPR–Cas complex to bind non-specific DNA[10], prevention of target DNA binding or cleavage[11] and many additional mechanisms[12–15]. Phage proteins and non-coding RNAs that inhibit toxin–antitoxin-mediated defence have also been described[16,17].

Whereas early research focused on restriction modification and later on CRISPR–Cas as the main mechanisms of defence against phage, recent studies exposed dozens of previously unknown defence systems that are widespread among bacteria and archaea[2,18–23]. These systems mediate defence by using a plethora of molecular mechanisms, including small-molecule signalling[20,24–28], production of antiviral compounds[22,29] and reverse transcription of non-coding RNAs[21,30]. Recently, several phage proteins that inhibit the bacterial cyclic oligonucleotide-based antiphage signalling system (CBASS) and Thoeris defence systems have been described[31–33]. However, it is still mostly unknown whether and how phages can overcome the wide variety of newly reported defence systems. In the current study we use comparative genomics of closely related phages to discover four distinct families of phage proteins that inhibit the Gabija, Thoeris and Hachiman defence systems.

Identification of anti-defence genes

In a previous study, we demonstrated that analysis of genomically similar phages that exhibit differential sensitivity to bacterial immunity enabled the discovery of a phage protein, called Tad1, that inhibits the Thoeris defence system[33]. To examine whether this methodology could be used to systematically detect anti-defence proteins within phages, we isolated and analysed several groups of closely related phages, and tested their sensitivity to several defence systems that protect *Bacillus* species from phage infection[18] (Fig. 1a). One group included eight newly isolated phages from the SPβ group, which also includes the previously isolated phages SPβ, phi3T and SPR[34–36]. These are temperate *Siphoviridae* phages with genomes of approximately 130 kilobases (kb) in length, with 43–96% alignable genomes when comparing phage pairs from this group (Extended Data Fig. 1a and Supplementary Tables 1 and 2). A second group included six phages similar to the phage SPO1, a lytic *Myoviridae* phage with an approximately 130-kb-long genome[37]. More than 85% of the genome was alignable when comparing phage pairs from this group, with high (80–99%) sequence identity in alignable regions (Fig. 1b and Supplementary Tables 3 and 4). The third group of phages included eight previously isolated phages from the SBSphiJ group, which were reported in a recent study[33] (Extended Data Fig. 1b and Supplementary Tables 5 and 6).

We next used this set of 25 phages to infect strains of *Bacillus subtilis* that expressed each of the defence systems described in ref. 18 as protecting against phages in *B. subtilis*. Five of these systems protected against at least one of the phages tested (Fig. 1c). However, phages

[1]Department of Molecular Genetics, Weizmann Institute of Science, Rehovot, Israel. [2]Department of Microbiology, Harvard Medical School, Boston, MA, USA. [3]Department of Cancer Immunology and Virology, Dana-Farber Cancer Institute, Boston, MA, USA. [4]Parker Institute for Cancer Immunotherapy at Dana-Farber Cancer Institute, Boston, MA, USA. [5]These authors contributed equally: Erez Yirmiya, Azita Leavitt. ✉e-mail: gil.amitai@weizmann.ac.il; rotem.sorek@weizmann.ac.il

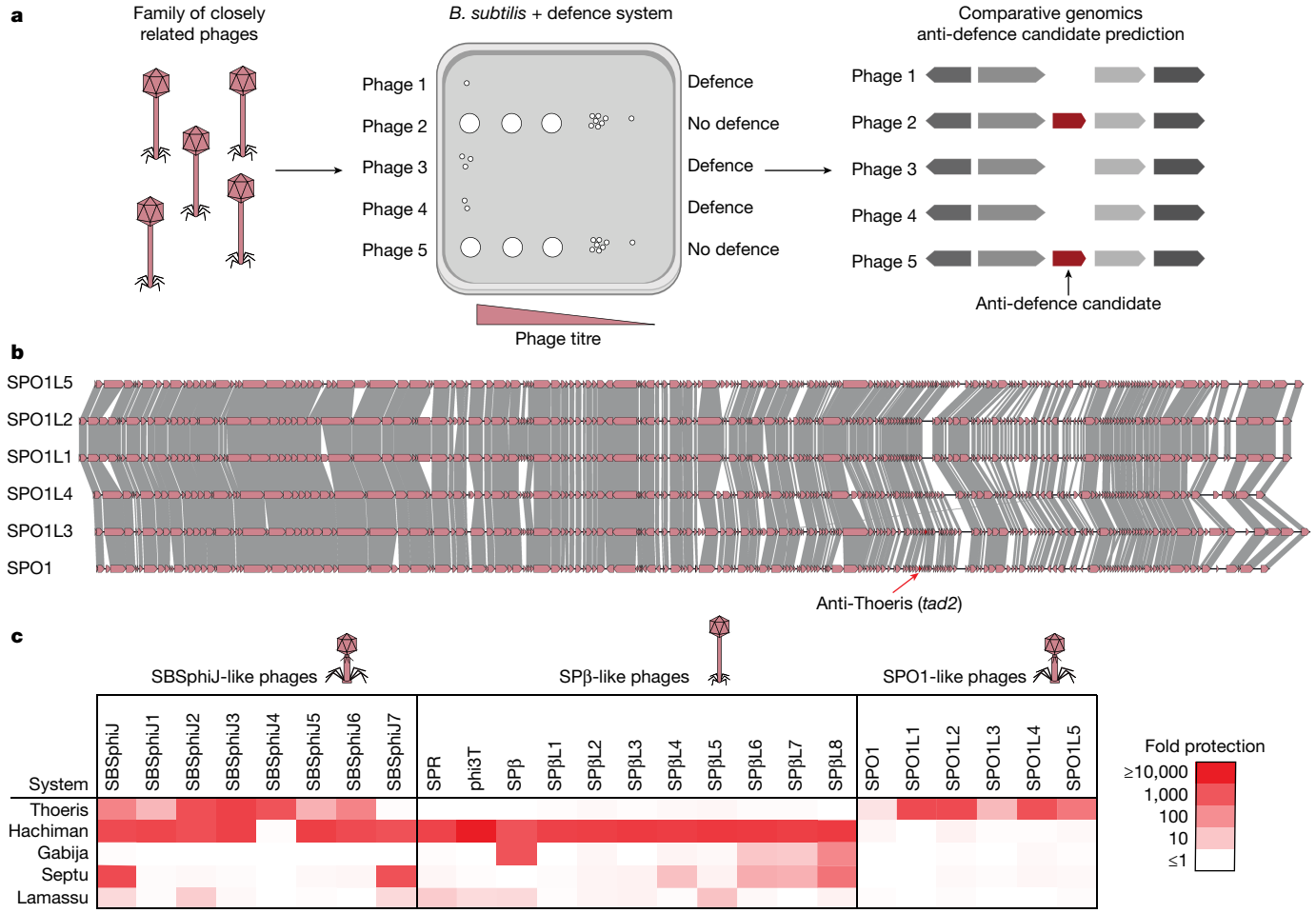

Fig. 1 | Identification of anti-defence genes based on differential sensitivity to defence systems. a, A flowchart of the experiments and analyses used in this study to detect candidate anti-defence genes. **b**, Genome comparison of six phages from the SPO1 group. Amino acid sequence similarity is marked by grey shading. Genome similarity was visualized using clinker[56]. **c**, Infection profile of SBSphiJ-like, SPβ-like and SPO1-like phages infecting five *B. subtilis* strains that express each of the defence systems Thoeris, Hachiman, Gabija, Septu and Lamassu. Fold defence was measured using serial dilution plaque assays, comparing the efficiency of plating of phages on the system-containing strain to the efficiency of plating on a control strain that lacks the systems and contains an empty vector instead. Data represent an average of three replicates. Detailed data from individual plaque assays are available in Extended Data Fig. 2.

from the same group exhibited remarkably different properties when infecting defence-system-containing bacteria. For example, the Gabija defence system provided strong protection against the phages SPβ and SPβL8 but not against other phages from the SPβ group such as SPR and phi3T; and the Hachiman defence system provided defence against all phages of the SBSphiJ group except SBSphiJ4 (Fig. 1c).

To identify phage genes that may explain the differential defence phenotype, we analysed the gene content in groups of phages that overcame each defence system and compared it to the gene content in phages that were blocked by the system. Genes common to phages that overcame the defence system, and not found in any of the phages that were blocked by the defence system, were considered as candidate anti-defence genes and were further examined experimentally.

Phage genes that inhibit Gabija

Gabija is a widespread bacterial defence system found in >15% of sequenced bacterial and archaeal genomes[38]. This system comprises two genes, *gajA* and *gajB*, which encode a DNA endonuclease and a UvrD-like helicase domain, respectively[18,39]. The Gabija system was shown to provide defence against a diverse set of phages[18,40].

The Gabija system from *Bacillus cereus* VD045, when cloned within *B. subtilis*, provided strong protection against some phages of the SPβ group including SPβ and SPβL8, and intermediate, weaker defence against the phages SPβL6 and SPβL7 (Fig. 1c and Extended Data Fig. 2a). The remaining seven phages of the SPβ group were able to completely overcome Gabija-mediated defence. We found two genes that were present in the seven Gabija-overcoming phages and missing from phages that were sensitive to Gabija defence (Fig. 2a, Extended Data Fig. 1a and Supplementary Table 7). One of these genes (open reading frame 129 (ORF129); Supplementary Table 7) did not show a Gabija-inhibiting phenotype when co-expressed with Gabija, and we were unable to clone the second gene (ORF128) into Gabija-expressing cells, presumably owing to toxicity. To examine the possible function of the non-cloned ORF128 gene, we knocked out that gene from the genome of the phage phi3T. Our results show that phi3T knocked out for ORF128 was no longer able to overcome Gabija defence, suggesting that this gene inhibits Gabija (Fig. 2b). We denote the anti-Gabija gene *gad1* (Gabija anti-defence 1). Engineering *gad1* from phi3T together with its native promoter into the genome of the phage SPβ, which naturally lacks this gene, rendered SPβ resistant to Gabija, confirming that *gad1* is both necessary and sufficient for the anti-Gabija phenotype (Fig. 2b).

Gad1 is a 295-amino-acid (aa)-long protein, which does not exhibit sequence similarity to proteins of known function. We found 94 homologues of Gad1, distributed in genomes of various phages and

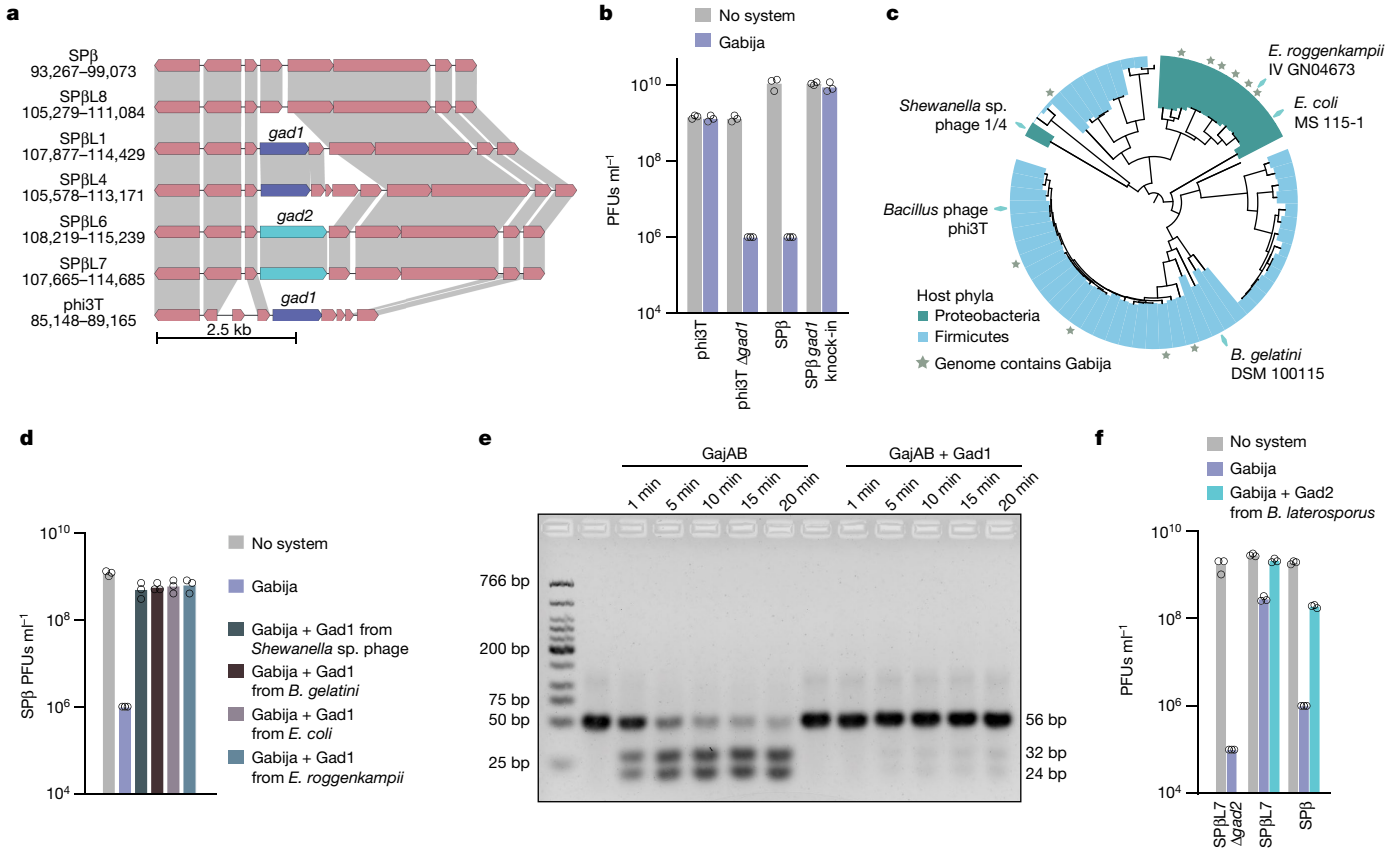

Fig. 2 | The Gad1 and Gad2 proteins inhibit Gabija defence. a, The anti-Gabija locus in phages of the SPβ group. Amino acid sequence similarity is marked by grey shading. Genome similarity was visualized using clinker[56]. **b**, Deletion of *gad1* from the phage phi3T eliminates the ability of the phage to cancel Gabija-mediated defence, and knock-in of *gad1* into the phage SPβ renders the phage resistant to Gabija. Data represent plaque-forming units (PFUs) per millilitre of phages infecting control cells (No system) and cells expressing the Gabija defence system. Shown is the average of three technical replicates, with individual data points overlaid. **c**, Phylogeny and distribution of Gad1 homologues. The names of bacteria in which Gad1 homologues were found in prophages and verified experimentally are indicated on the tree by cyan diamonds. **d**, Results of phage infection experiments. Data represent PFUs per millilitre of SPβ infecting control cells (No system), cells expressing the Gabija system (Gabija) and cells co-expressing the Gabija system and a Gad1 homologue. Shown is the average of three technical replicates, with individual data points overlaid. **e**, Gad1 blocks Gabija-mediated DNA cleavage. Incubation of purified Gabija (GajAB) complex, or Gabija co-purified with Gad1 from the *Shewanella* sp. phage 1/4 (GajAB + Gad1) with a previously described DNA substrate from the phage lambda[39]. Shown is a representative agarose gel from three independent experiments of proteins with 1-, 5-, 10-, 15- or 20-min incubation with DNA. **f**, Knockout of *gad2* from the phage SPβL7 renders the phage sensitive to Gabija defence, and expression of a Gad2 homologue from a *B. laterosporus* prophage allows SPβ to overcome Gabija-mediated defence. Phage infection experiments were conducted as in **d**.

prophages infecting host bacteria from the phyla *Proteobacteria* and *Firmicutes* (Fig. 2c and Supplementary Tables 8 and 9). Notably, many of the Gad1-containing prophages were integrated in bacterial genomes that also encoded the Gabija system, suggesting that Gad1 enabled these phages to overcome Gabija-mediated defence of their hosts (Fig. 2c). Five Gad1 homologues from phages infecting *Shewanella* sp., *Enterobacter roggenkampii*, *Escherichia coli*, *Brevibacillus gelatini* and *Bacillus xiamenensis* were selected for further experimental examination as representatives of the phylogenetic diversity of the Gad1 family (Fig. 2c and Extended Data Fig. 3a). Unlike the Gad1 protein from the phage phi3T, four of the Gad1 homologues were not toxic when expressed in Gabija-containing cells (all except the homologue cloned from the *B. xiamenensis* prophage). Each of these four homologues efficiently inhibited Gabija defence when co-expressed in Gabija-containing cells (Fig. 2d and Extended Data Fig. 3b).

It was recently shown that Gabija identifies and cleaves DNA having a specific nearly palindromic sequence motif derived from the phage lambda[39]. By purifying GajA and GajB and reconstituting the Gabija complex in vitro, we were able to confirm that Gabija cleaves DNA that contains the specific sequence motif (Fig. 2e). Gabija purified in the presence of Gad1 was unable to cleave DNA (Fig. 2e). In a companion paper, we show that Gad1 binds the Gabija complex as an octamer and inhibits its ability to bind and cleave DNA[41].

We next examined the phages SPβL6 and SPβL7, which lack *gad1* but were still partially resistant to Gabija (Fig. 1c). Notably, these phages encoded, at the same locus where *gad1* was encoded in other phages, another gene of unknown function. Knocking out this gene from the phage SPβL7 rendered this phage completely sensitive to Gabija (Fig. 2f). The gene from SPβL7 was toxic when expressed in bacteria, but co-expression of a non-toxic homologue from a prophage of *Brevibacillus laterosporus* with Gabija completely inhibited Gabija defence, further verifying that it is an anti-Gabija gene, which we denote here as *gad2* (Fig. 2a,f). Gad2 is a 400-aa-long protein that shows no sequence similarity to Gad1 or to other known proteins. Homology searches identified 170 homologues of Gad2 that almost always reside in genomes of phages and prophages infecting diverse host bacteria (Extended Data Fig. 4a and Supplementary Tables 10 and 11). Notably, structural analysis using Alphafold2[42] predicted that Gad2 is an enzyme with a nucleotidyltransferase protein domain, suggesting that it inhibits Gabija through a mechanism of action different from that of Gad1 (Extended Data Fig. 4b). Point mutations in residues predicted to form the active site of the *B. laterosporus* Gad2 nucleotidyltransferase domain rendered Gad2

inactive, suggesting that nucleotidyltransferase activity is necessary for the anti-defence function (Extended Data Fig. 4c). Purified *B. laterosporus* Gad2 did not bind the Gabija complex in vitro and did not inhibit DNA cleavage, implying that Gad2 may operate upstream to Gabija to modify the phage molecules sensed by the GajA–GajB defence complex (Extended Data Fig. 4d–f). Combined together, our results suggest that SPβ-like phages encode anti-Gabija genes in a dedicated locus in their genomes, where multiple different Gabija-inhibiting genes can reside.

Phage genes that inhibit Thoeris

The Thoeris defence system is present in approximately 4% of sequenced bacterial and archaeal genomes[18]. This system encodes ThsB, a protein with a Toll/interleukin-1 receptor (TIR) domain that serves as a sensor for phage infection, and ThsA, an NAD^+-cleaving protein[27]. Following phage recognition, the Thoeris ThsB protein generates 1″–3′ gcADPR, a signalling molecule that activates ThsA, resulting in the depletion of NAD^+ and the inhibition of phage replication[33].

Our recent discovery of the anti-Thoeris gene *tad1*, a 1″–3′ gcADPR sponge present in the phage SBSphiJ7 and absent from other phages in the SBSphiJ group, explains the observed insensitivity of SBSphiJ7 to Thoeris[33] (Fig. 1c and Extended Data Fig. 2c). We reasoned that the phages SPO1 and SPO1L3 may also encode homologues of *tad1*, as these phages partially escaped Thoeris-mediated defence (Fig. 1c and Extended Data Fig. 2b), but we were unable to identify *tad1* homologues in these phages. Instead, we identified a single gene present in SPO1 and SPO1L3 but absent from all other Thoeris-sensitive SPO1-like phages (Fig. 3a and Supplementary Table 7). We expressed this gene, designated here as *tad2*, within *B. subtilis* cells that also express the Thoeris system from *B. cereus* MSX-D12. Tad2 robustly inhibited the activity of Thoeris, allowing Thoeris-sensitive phages to infect Thoeris-expressing cells (Fig. 3b). Moreover, engineering *tad2* into SBSphiJ, a phage that is normally blocked by Thoeris, resulted in a phage that overcomes Thoeris-mediated defence (Fig. 3b). Silencing the expression of Tad2 in SPO1 using dead Cas9 (dCas9; ref. 43) further confirmed that Tad2 is responsible for the Thoeris-inhibiting phenotype of SPO1 (Fig. 3c).

Tad2 is a short protein (89 aa) containing a DUF2829 protein domain. Sequence homology searches identified more than 650 homologues in the Integrated Microbial Genomes[44] and Metagenomic Gut Virus[45] databases (Supplementary Tables 12 and 13). Phylogenetic analysis revealed that Tad2 is encoded by phages belonging to several phage morphology groups, including *Myoviridae*, *Podoviridae* and *Siphoviridae*, as well as by prophages integrated within more than 100 bacterial species from 6 different phyla (Fig. 3d). We selected five Tad2 homologues representing the phylogenetic diversity of the family and cloned each one separately into *B. subtilis* cells expressing the Thoeris system (Fig. 3d and Extended Data Fig. 5a). Four of these Tad2 homologues were able to inhibit Thoeris, including homologues derived from phages infecting distant organisms such as *Ruminococcus callidus* and *Maridesulfovibrio bastinii* (Extended Data Fig. 5b). These results demonstrate that Tad2 represents a large family of proteins used by phages to inhibit the Thoeris defence system.

During phage infection, ThsB generates the 1″–3′ gcADPR signalling molecule to activate ThsA[33]. As expected, purified ThsA incubated with filtered cell lysates derived from SBSphiJ-infected, ThsB-expressing cells became a strong NADase, indicating that ThsB produced 1″–3′ gcADPR in response to SBSphiJ infection as previously shown[33] (Fig. 4a). However, filtered lysates from similarly infected cells that co-expressed both ThsB and Tad2 failed to activate ThsA in vitro, suggesting that Tad2 functions upstream of ThsA (Fig. 4a).

Recent studies have shown that phages can use dedicated proteins to degrade[32,46] or sequester[31,33] bacterial immune signalling molecules. Incubation of Tad2 with 1″–3′ gcADPR in vitro did not yield observable degradation products, suggesting that Tad2 is not an enzyme that cleaves 1″–3′ gcADPR (Extended Data Fig. 6a). To test whether Tad2 might act as a sponge that binds and sequesters the immune signal, we incubated purified Tad2 with 1″–3′ gcADPR, and then heated the reaction at 95 °C to denature Tad2. The denatured reaction readily activated ThsA, suggesting that Tad2 functions by binding and sequestering the Thoeris-derived signalling molecule, and that denaturation of Tad2 released the intact molecule back to the medium (Fig. 4b). In support of this observation, our size-exclusion chromatography results showed that Tad2 that was pre-incubated with 1″–3′ gcADPR exhibited a substantial mobility shift (Extended Data Fig. 6b). In addition, Tad2 exhibited an increased absorption ratio of UV_{260nm}/UV_{280nm} following incubation with 1″–3′ gcADPR, further confirming that Tad2 binds this molecule as a ligand (Extended Data Fig. 6b). We found that Tad2 binds 1″–3′ gcADPR with an equilibrium dissociation constant (K_D) of 23.3 nM (Extended Data Fig. 6c). Notably, Tad2 could not bind the canonical cADPR, demonstrating high specificity of Tad2 to the ThsB-derived signalling molecule (Extended Data Fig. 6d).

To define the mechanism of 1″–3′ gcADPR sequestration and Thoeris inhibition, we determined crystal structures of Tad2 from the phage SPO1 in the apo and 1″–3′ gcADPR ligand-bound states (Extended Data Table 1). We also determined crystal structures of Tad2 bound to 1″–2′ gcADPR and Tad1 from a prophage of *Clostridium botulinum* bound to 1″–3′ gcADPR (Extended Data Table 1). The structures of Tad2 reveal a homotetrameric assembly consistent with oligomerization observed during size-exclusion chromatography analysis (Extended Data Fig. 7). Two Tad2 protomers pack together at helix α2 and sheet β2 to form V-shaped homodimeric units, which then interlock perpendicularly along helix α1 to complete tetramerization (Fig. 4c and Extended Data Fig. 8). The resulting assembly creates two identical ligand-binding pockets formed at the interface of two adjacent non-dimeric protomers, surrounded by loop β1–β2, loop β3–β4 and strand β4 of one protomer, and loop β1–β2, loop β4–α3 and helix α3 of the other (Fig. 4c–f).

A 1.75-Å structure of Tad2 in complex with 1″–3′-gcADPR explains the molecular basis of signal recognition. In the Tad2–1″–3′-gcADPR complex, ligand binding is mediated by extensive van der Waals interactions from $W25_{a,b}$ and $W73_{a,b}$, as well as polar interactions to phosphates and free hydroxyls from $N26_{a,b}$ and $D79_{a,b}$ (Fig. 4e,f). Compared to the Tad1–1″–3′-gcADPR complex, Tad2 forms very few contacts to the adenine base of 1″–3′ gcADPR, with one hydrogen bond from $T78_b$ and nonpolar interactions from $I63_a$ and $T65_a$, whereas Tad1 forms base-stacking interactions via $F82_b$ and $R109_a$, as well as specific hydrogen bonding to the Hoogsteen edge via $N92_b$ (Fig. 4e,f and Extended Data Fig. 8). Additionally, we observed several key water molecules in the Tad2 structure that contribute to 1″–3′ gcADPR binding and are coordinated by $N26_b$, $D67_a$, $H71_a$, $W73_b$, $S76_b$ and $D79_{a,b}$ (Fig. 4e,f). Tad2 binds both 1″–3′ gcADPR and 1″–2′ gcADPR via the same binding residues, and both molecules are oriented nearly identically in the Tad2 binding pocket (Extended Data Fig. 8b,c). Although the molecular basis for ligand recognition is dissimilar between Tad2 and Tad1, we observe that Tad1, too, binds both 1″–3′ gcADPR and 1″–2′ gcADPR in the same pocket and orientation (Extended Data Fig. 8e,f), highlighting how both proteins function as sponges for gcADPR molecules. Taken together, our findings show that Tad2 inhibits Thoeris defence by binding and sequestering 1″–3′ gcADPR, preventing the activation of the Thoeris immune effector and mitigating Thoeris-mediated defence.

Phage genes that inhibit Hachiman

Hachiman is a defence system whose mechanism of action remains unsolved. It encodes a protein with a predicted helicase domain, as well as an additional protein with no known functional domains. Hachiman is found in more than 3% of sequenced bacterial and archaeal genomes, and was shown to provide strong protection against a broad range of phages[18].

We cloned three short genes that were unique to the phage SBSphiJ4, a phage that overcame Hachiman-mediated defence (Fig. 1c and Supplementary Table 7), into a *B. subtilis* strain that expresses the Hachiman

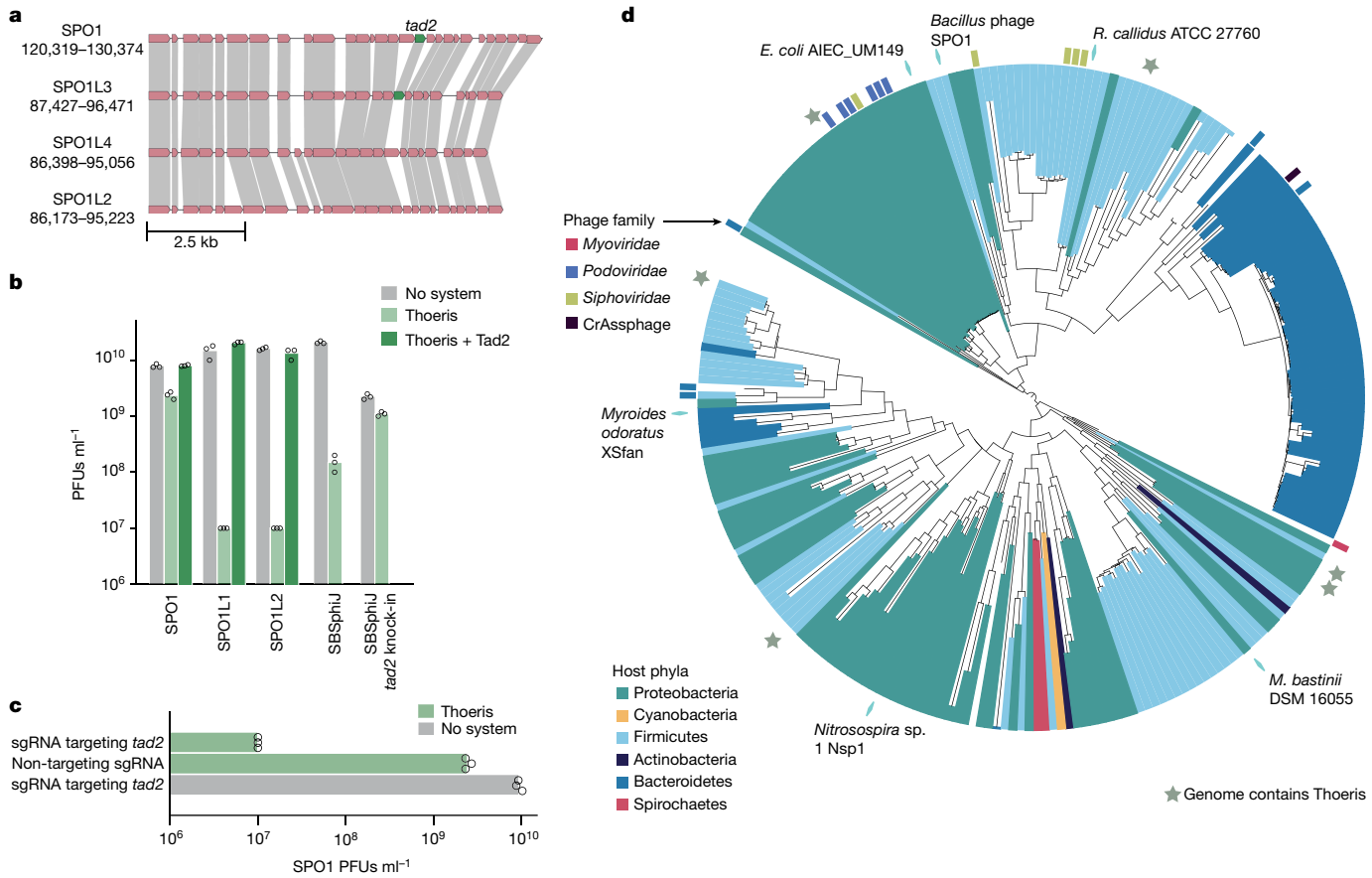

Fig. 3 | Tad2 proteins inhibit Thoeris defence. a, The genomic locus of the anti-Thoeris gene *tad2* in the phages SPO1 and SPO1L3, and the respective locus in the phages SPO1L4 and SPO1L2. Amino acid sequence similarity is marked by grey shading. Genome similarity was visualized using clinker[56]. **b**, Anti-Thoeris activity of Tad2. Data represent PFUs per millilitre of phages infecting control cells (No system), cells expressing the Thoeris system (Thoeris) and cells co-expressing the Thoeris system and the *tad2* gene from SPO1 (Thoeris + Tad2). Data for the phage SBSphiJ as well as for SBSphiJ with a *tad2* knock-in are also presented. Shown is the average of three technical replicates, with individual data points overlaid. **c**, *tad2* knockdown cancels anti-Thoeris activity. Data represent PFUs per millilitre of SPO1 that infects cells expressing Thoeris and a dCas9 system targeting *tad2*, as well as control cells. Shown is the average of three technical replicates, with individual data points overlaid. **d**, Phylogenetic analysis of Tad2 homologues in phage and prophage genomes. The names of bacteria in which Tad2 homologues were found in prophages and tested experimentally are indicated on the tree by cyan diamonds.

system from *B. cereus* B4087 (ref. 18). One of these genes completely abolished Hachiman-mediated defence, and we therefore named it *had1* (Hachiman anti-defence 1) (Fig. 5a,b). Silencing of Had1 expression in SBSphiJ4 resulted in a phage that could infect control strains, but was blocked by Hachiman defence (Fig. 5c). In addition, SBSphiJ that was engineered to include Had1 with its native promoter was able to overcome Hachiman defence, demonstrating that Had1 is responsible for the anti-Hachiman phenotype (Fig. 5b).

Had1 is a short protein of 53 aa in size, which does not show sequence homology to any protein of known function. We found 23 homologues of Had1 in *Bacillus* phages as well as prophages integrated within *Bacillus* and *Paenibacillus* genomes (Supplementary Table 17), and selected five homologues that span the protein sequence diversity of Had1 for further experimental examination. Four of these proteins efficiently inhibited the activity of Hachiman, and we could not clone the fifth into Hachiman-expressing cells, possibly owing to toxicity (Extended Data Fig. 9a,b). These results confirm that Had1 is a Hachiman-inhibiting family of phage proteins.

We determined the crystal structure of Had1 from *Bacillus toyonensis*, revealing a homodimeric complex with two splayed loops that form an overall platform-like shape (Fig. 5d and Extended Data Fig. 9c,d). The Had1 dimeric interface consists of four β-strands, two contributed by each protomer (Fig. 5d). At the centre of the Had1 complex platform there is a positively charged patch formed by conserved residues in strand β2 including R17 and K18 (Fig. 5e). A Had1 residue I41 at the centre of the dimeric interface in each protomer forms hydrophobic packing interactions with five residues on the other protomer, supporting the dimerization interface (Fig. 5f). Substitution of the equivalent isoleucine residue in SBSphiJ4 Had1 rendered the protein unable to inhibit Hachiman, suggesting that the dimeric structure is necessary for Had1 evasion of host antiphage defence (Fig. 5g).

It was previously shown that the SBSphiJ phage can escape Hachiman defence by mutating its single-stranded-DNA-binding protein, and it was suggested that Hachiman may recognize protein–DNA complexes produced as an intermediate of phage DNA replication or recombination[40]. The positively charged patch at the centre of the Had1 dimeric complex (Fig. 5e) may imply that Had1 might shield phage replication intermediates from being recognized by the Hachiman system. As the mechanism of Hachiman defence is unknown at present, understanding how Had1 inhibits Hachiman in future studies may assist in solving the mechanism of Hachiman defence.

In this study, we identified multiple families of phage anti-defence proteins using comparative analysis of closely related phage genomes. Our findings demonstrate that phages have evolved diverse strategies to counter the complex, multilayered bacterial defence arsenal. Our data suggest that SPβ-like phages store anti-Gabija genes in a dedicated anti-Gabija locus in their genomes. This is reminiscent of anti-CRISPR loci identified in phages of *Pseudomonas* and other species, where

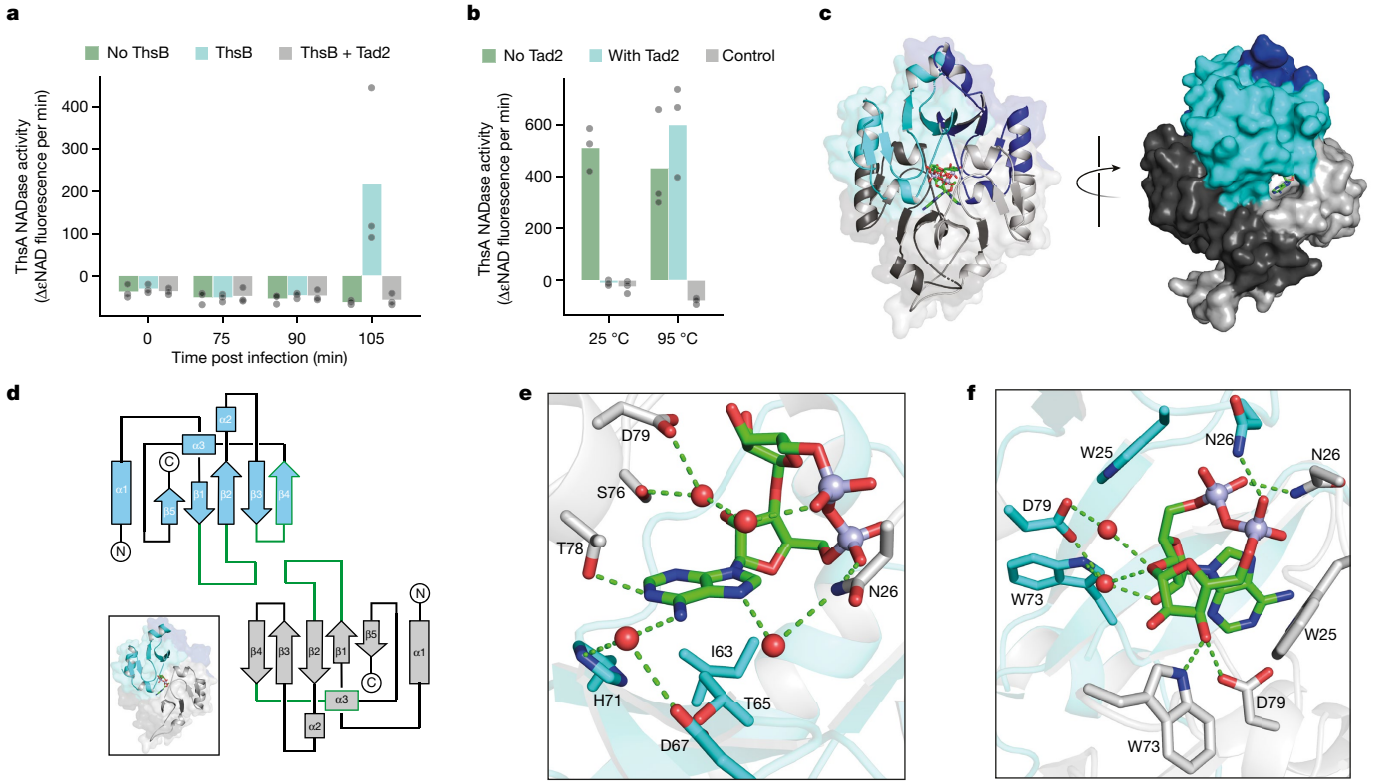

Fig. 4 | Tad2 cancels Thoeris-mediated defence by sequestering 1″–3′ gcADPR. **a**, Cells expressing ThsB or both ThsB and Tad2 or control cells that do not express ThsB were infected with the phage SBSphiJ at a multiplicity of infection of 10. The NADase activity of purified ThsA incubated with filtered lysates was measured using a nicotinamide 1,N^6-ethenoadenine dinucleotide (εNAD) cleavage fluorescence assay. Bars represent the mean of three experiments, with individual data points overlaid. **b**, Tad2 releases bound 1″–3′ gcADPR when denatured. Shown is the NADase activity of purified ThsA incubated with 600 nM 1″–3′ gcADPR that was pre-incubated with 2.4 μM of purified Tad2 in vitro for 10 min, followed by an additional incubation of 10 min at either 25 °C or 95 °C. Control is buffer without 1″–3′ gcADPR. Bars represent the mean of three experiments, with individual data points overlaid. **c**, Overview of the crystal structure of Tad2 in complex with 1″–3′ gcADPR in cartoon (front) and surface (side) representation. Tad2 exists as a homotetramer formed by two dimer units (coloured cyan with dark blue and grey with dark grey). Non-dimeric monomer pairs form two recessed ligand-binding pockets that enclose 1″–3′ gcADPR. **d**, Topology map of two Tad2 monomers that come together to form the ligand-binding pocket. Components that form the binding pocket are outlined in green. Each dimer subunit donates one monomer, as shown by the cartoon representation. **e**,**f**, Detailed views centred around the adenine base (**e**) or ribose and phosphates (**f**) of residues that either directly interact with 1″–3′ gcADPR or coordinate key water molecules that reside within the binding pocket. Residues contributed by each of the two monomers that form the binding pocket are represented in cyan ($Tad2_a$) or grey ($Tad2_b$).

different sets of anti-CRISPR genes are present in each individual phage[47]. Our discovery of a specific anti-Gabija locus in SPβ-like phages may point to a general rule for the organization of anti-defence genes in phage genomes, a genomic phenomenon that can assist in future searches for anti-defence genes.

The most widely distributed family of anti-defence proteins discovered here is that of Tad2, a protein that contains a domain of unknown function, DUF2829. A protein with DUF2829 was previously speculated to inhibit type II CRISPR–Cas systems and specifically Cas9 (ref. 48), although binding to Cas9 was not demonstrated and the mechanism through which this protein antagonizes type II CRISPR–Cas was not determined[48]. Our findings that multiple DUF2829-containing proteins antagonize the Thoeris defence system by specifically binding and sequestering 1″–3′ gcADPR suggest that the DUF2829 family of proteins represent anti-Thoeris proteins rather than anti-CRISPR proteins.

Our results on Tad2 join recent discoveries of additional anti-defence proteins that function by sequestering immune signalling molecules[31,33]. These include Tad1, a completely different family of Thoeris-inhibiting proteins, which, similar to Tad2, also bind and sequester gcADPR molecules; and the phage-encoded Acb2 protein that inhibits CBASS defence by binding the cyclic oligonucleotide immune signalling molecules produced by CBASS[31,33]. It therefore seems that the production of protein 'sponges' that sequester immune signalling molecules is a highly efficient strategy that evolved within phages multiple times in parallel to allow successful evasion of immune systems that utilize immune signalling molecules. The efficiency of this strategy may be perceived as counterintuitive, because it necessitates a 1:1 ratio between the number of phage sponge proteins and the immune signalling molecule (or even 2:1 in the case of Tad2). However, as Thoeris and CBASS become active and produce the immune signalling molecule relatively late in the infection cycle of the phage[20,27], phages have sufficient time to express a substantial amount of their sponge proteins at the early stages of infection. Thus, when the immune signalling molecule is produced by the defence system, there will already be enough copies of the sponge protein in the infected cell to efficiently block immune signalling. An alternative explanation for the efficiency of phage sponges could be that they have a higher affinity to the signalling molecule as compared to the bacterial effector. The affinity we measured for Tad2 binding to 1″–3′ gcADPR (K_D = 23.3 nM; Extended Data Fig. 6c) is indeed higher than the affinity measured for binding of the same molecule to Thoeris ThsA (K_D = 59.1 nM)[49], but both are within the same order of magnitude of nanomolar affinity.

We were not able to identify inhibitors of the Septu or Lamassu defence systems among the three groups of phages that we studied, although phages from these groups exhibited differential sensitivity to these defence systems. It is possible that escape from these two systems is mediated by mutations in existing genes rather than the presence of a dedicated anti-defence gene[40]. It is also possible that different phages in the same group utilize more than one protein to

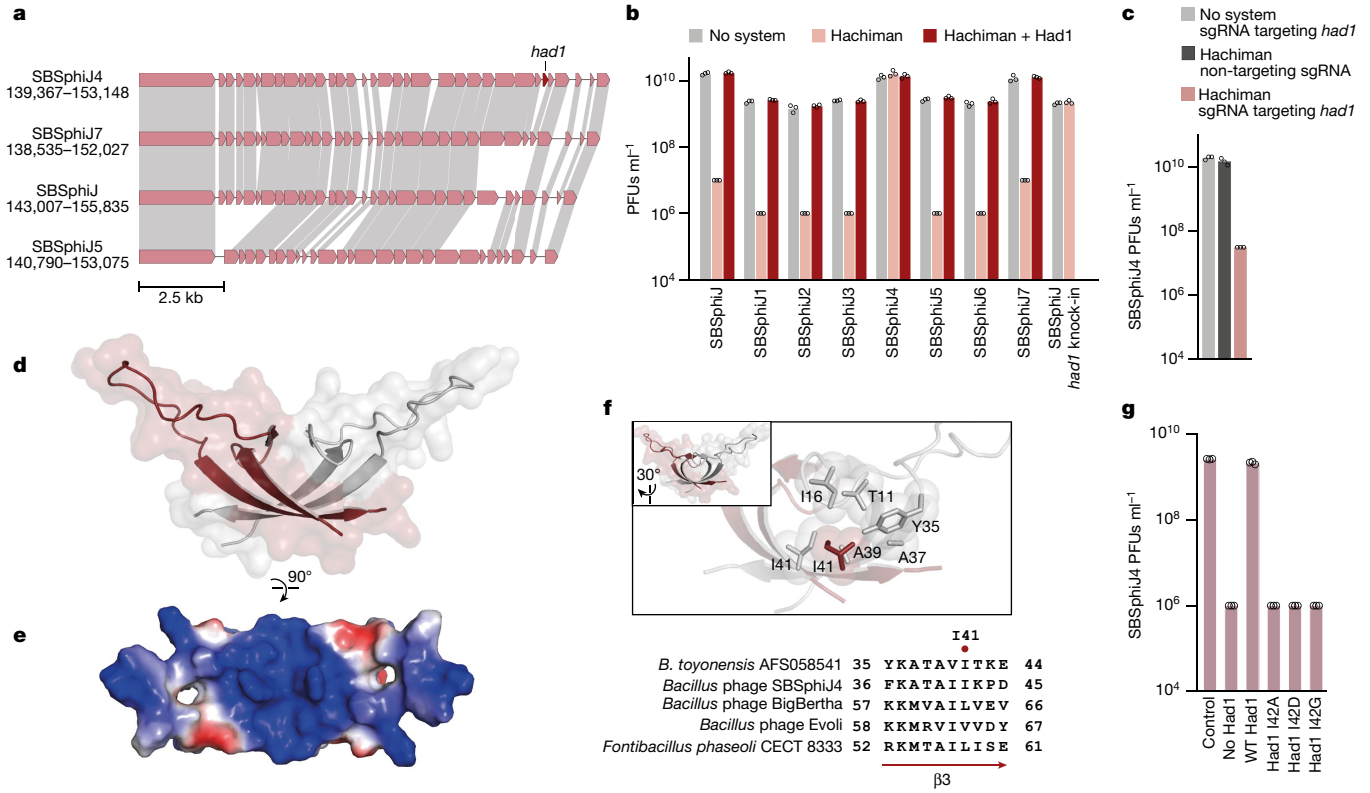

Fig. 5 | Had1 proteins inhibit Hachiman defence. a, The genomic locus of the anti-Hachiman gene *had1* in the phage SBSphiJ4, as well as the relevant locus in the phages SBSphiJ7, SBSphiJ and SBSphiJ5. Amino acid sequence similarity is marked by grey shading. Genome similarity was visualized using clinker[56]. **b**, Differential defence of Hachiman against phages from the SBSphiJ group, and anti-Hachiman activity of Had1. Data represent PFUs per millilitre of phages infecting control cells (No system), cells expressing the Hachiman system (Hachiman) and cells co-expressing the Hachiman system and the *had1* gene from SBSphiJ4 (Hachiman + Had1). Data for the phage SBSphiJ with a *had1* knock-in are also presented. Shown is the average of three technical replicates, with individual data points overlaid. **c**, *had1* knockdown cancels anti-Hachiman activity. Results of the phage SBSphiJ4 infection experiments. Data represent PFUs per millilitre of SBSphiJ4 infecting cells expressing Hachiman and a dCas9 with an sgRNA targeting *had1*, as well as control cells. Shown is the average of three technical replicates, with individual data points overlaid. **d**,**e**, *B. toyonensis* Had1 structure overview (**d**) and surface electrostatics (**e**). Had1 is a homodimer (coloured red and light grey) with a central β-barrel core formed by strands β1–β3 and splayed loops that create a complex with an overall platform-like shape. **f**, Zoomed-in cutaway (top) and sequence alignment (bottom) of the *B. toyonensis* Had1 residue I41 that forms hydrophobic packing interactions with T11, I16, Y35, A37 and A39 from the opposing protomer. **g**, Had1 alterations at the centre of the dimeric interface result in loss of anti-defence activity. Data represent PFUs per millilitre of the phage SBSphiJ infecting cells that co-express the Hachiman system and WT or mutated Had1 from phage SBSphiJ4, as well as control cells lacking Had1 and control cells lacking both Had1 and Hachiman. Shown is the average of three technical replicates, with individual data points overlaid.

overcome defence, which would sometime hamper the analysis pipeline used in this study.

With the emergence of antibiotic-resistant bacteria[50], phage therapy, in which phages are used as an alternative to antibiotics, is being considered as a suitable therapeutic avenue for defeating bacterial pathogens[51–53]. One of the major obstacles for successful phage therapy is the recently discovered ability of bacteria to actively defend themselves by encoding a large variety of defence systems. Indeed, it was shown that the set of defence systems carried by a given bacterial strain is a strong determinant for the susceptibility of that strain to phages[54,55]. Engineering phages to carry a set of anti-defence proteins can enable them to overcome bacterial defences, resulting in phages with increased host ranges that will be more suitable for phage therapy. Thus, the anti-defence proteins we discovered here, as well as additional such proteins that were discovered and will be discovered in the future, could be used as tools for more efficient phage therapy applications.

Online content

Any methods, additional references, Nature Portfolio reporting summaries, source data, extended data, supplementary information, acknowledgements, peer review information; details of author contributions and competing interests; and statements of data and code availability are available at https://doi.org/10.1038/s41586-023-06869-w.

1. Dy, R. L., Richter, C., Salmond, G. P. C. & Fineran, P. C. Remarkable mechanisms in microbes to resist phage infections. *Annu. Rev. Virol.* **1**, 307–331 (2014).
2. Bernheim, A. & Sorek, R. The pan-immune system of bacteria: antiviral defence as a community resource. *Nat. Rev. Microbiol.* **18**, 113–119 (2020).
3. Hampton, H. G., Watson, B. N. J. & Fineran, P. C. The arms race between bacteria and their phage foes. *Nature* **577**, 327–336 (2020).
4. Tal, N. & Sorek, R. SnapShot: bacterial immunity. *Cell* **185**, 578 (2022).
5. Samson, J. E., Magadán, A. H., Sabri, M. & Moineau, S. Revenge of the phages: defeating bacterial defences. *Nat. Rev. Microbiol.* **11**, 675–687 (2013).
6. Atanasiu, C., Su, T.-J., Sturrock, S. S. & Dryden, D. T. F. Interaction of the ocr gene 0.3 protein of bacteriophage T7 with EcoKI restriction/modification enzyme. *Nucleic Acids Res.* **30**, 3936–3944 (2002).
7. Walkinshaw, M. et al. Structure of Ocr from bacteriophage T7, a protein that mimics B-form DNA. *Mol. Cell* **9**, 187–194 (2002).
8. Drozdz, M., Piekarowicz, A., Bujnicki, J. M. & Radlinska, M. Novel non-specific DNA adenine methyltransferases. *Nucleic Acids Res.* **40**, 2119–2130 (2012).
9. Thavalingam, A. et al. Inhibition of CRISPR-Cas9 ribonucleoprotein complex assembly by anti-CRISPR AcrIIC2. *Nat. Commun.* **10**, 2806 (2019).
10. Lu, W.-T., Trost, C. N., Müller-Esparza, H., Randau, L. & Davidson, A. R. Anti-CRISPR AcrIF9 functions by inducing the CRISPR–Cas complex to bind DNA non-specifically. *Nucleic Acids Res.* **49**, 3381–3393 (2021).
11. Bondy-Denomy, J. et al. Multiple mechanisms for CRISPR–Cas inhibition by anti-CRISPR proteins. *Nature* **526**, 136–139 (2015).
12. Stanley, S. Y. & Maxwell, K. L. Phage-encoded anti-CRISPR defenses. *Annu. Rev. Genet.* **52**, 445–464 (2018).

13. Li, Y. & Bondy-Denomy, J. Anti-CRISPRs go viral: the infection biology of CRISPR-Cas inhibitors. *Cell Host Microbe* **29**, 704–714 (2021).
14. Jia, N. & Patel, D. J. Structure-based functional mechanisms and biotechnology applications of anti-CRISPR proteins. *Nat. Rev. Mol. Cell Biol.* **22**, 563–579 (2021).
15. Davidson, A. R. et al. Anti-CRISPRs: protein inhibitors of CRISPR-Cas systems. *Annu. Rev. Biochem.* **89**, 309–332 (2020).
16. Otsuka, Y. & Yonesaki, T. Dmd of bacteriophage T4 functions as an antitoxin against *Escherichia coli* LsoA and RnlA toxins. *Mol. Microbiol.* **83**, 669–681 (2012).
17. Blower, T. R., Evans, T. J., Przybilski, R., Fineran, P. C. & Salmond, G. P. C. Viral evasion of a bacterial suicide system by RNA–based molecular mimicry enables infectious altruism. *PLoS Genet.* **8**, e1003023 (2012).
18. Doron, S. et al. Systematic discovery of antiphage defense systems in the microbial pangenome. *Science* **359**, eaar4120 (2018).
19. Gao, L. et al. Diverse enzymatic activities mediate antiviral immunity in prokaryotes. *Science* **369**, 1077–1084 (2020).
20. Cohen, D. et al. Cyclic GMP–AMP signalling protects bacteria against viral infection. *Nature* **574**, 691–695 (2019).
21. Millman, A. et al. Bacterial retrons function in anti-phage defense. *Cell* **183**, 1551–1561 (2020).
22. Bernheim, A. et al. Prokaryotic viperins produce diverse antiviral molecules. *Nature* **589**, 120–124 (2021).
23. Millman, A. et al. An expanded arsenal of immune systems that protect bacteria from phages. *Cell Host Microbe* **30**, 1556–1569 (2022).
24. Whiteley, A. T. et al. Bacterial cGAS-like enzymes synthesize diverse nucleotide signals. *Nature* **567**, 194–199 (2019).
25. Lau, R. K. et al. Structure and mechanism of a cyclic trinucleotide-activated bacterial endonuclease mediating bacteriophage immunity. *Mol. Cell* **77**, 723–733 (2020).
26. Millman, A., Melamed, S., Amitai, G. & Sorek, R. Diversity and classification of cyclic-oligonucleotide-based anti-phage signalling systems. *Nat. Microbiol.* **5**, 1608–1615 (2020).
27. Ofir, G. et al. Antiviral activity of bacterial TIR domains via immune signalling molecules. *Nature* **600**, 116–120 (2021).
28. Tal, N. et al. Cyclic CMP and cyclic UMP mediate bacterial immunity against phages. *Cell* **184**, 5728–5739 (2021).
29. Kronheim, S. et al. A chemical defence against phage infection. *Nature* **564**, 283–286 (2018).
30. Bobonis, J. et al. Bacterial retrons encode phage-defending tripartite toxin–antitoxin systems. *Nature* **609**, 144–150 (2022).
31. Huiting, E. et al. Bacteriophages inhibit and evade cGAS-like immune function in bacteria. *Cell* **186**, 864–876 (2023).
32. Hobbs, S. J. et al. Phage anti-CBASS and anti-Pycsar nucleases subvert bacterial immunity. *Nature* **605**, 522–526 (2022).
33. Leavitt, A. et al. Viruses inhibit TIR gcADPR signalling to overcome bacterial defence. *Nature* **611**, 326–331 (2022).
34. Rosenthal, R., Toye, P. A., Korman, R. Z. & Zahler, S. A. The prophage of SP beta c2dcitK1, a defective specialized transducing phage of *Bacillus subtilis*. *Genetics* **92**, 721–739 (1979).
35. Tucker, R. G. Acquisition of thymidylate synthetase activity by a thymine-requiring mutant of *Bacillus subtilis* following Infection by the temperate phage φ3. *J. Gen. Virol.* **4**, 489–504 (1969).
36. Noyer-Weidner, M., Jentsch, S., Pawlek, B., Günthert, U. & Trautner, T. A. Restriction and modification in *Bacillus subtilis*: DNA methylation potential of the related bacteriophages Z, SPR, SP beta, phi 3 T, and rho 11. *J. Virol.* **46**, 446–453 (1983).
37. Stewart, C. R. et al. The genome of *Bacillus subtilis* bacteriophage SPO1. *J. Mol. Biol.* **388**, 48–70 (2009).
38. Tesson, F. et al. Systematic and quantitative view of the antiviral arsenal of prokaryotes. *Nat. Commun.* **13**, 2561 (2022).
39. Cheng, R. et al. A nucleotide-sensing endonuclease from the Gabija bacterial defense system. *Nucleic Acids Res.* **49**, 5216–5229 (2021).
40. Stokar-Avihail, A. et al. Discovery of phage determinants that confer sensitivity to bacterial immune systems. *Cell* **186**, 1863–1876 (2023).
41. Antine, S. P. et al. Structural basis of Gabija anti-phage defense and viral immune evasion. *Nature* https://doi.org/10.1038/s41586-023-06855-2 (2023).
42. Jumper, J. et al. Highly accurate protein structure prediction with AlphaFold. *Nature* **596**, 583–589 (2021).
43. Peters, J. M. et al. A comprehensive, CRISPR-based functional analysis of essential genes in bacteria. *Cell* **165**, 1493–1506 (2016).
44. Chen, I.-M. A. et al. IMG/M v.5.0: an integrated data management and comparative analysis system for microbial genomes and microbiomes. *Nucleic Acids Res.* **47**, D666–D677 (2019).
45. Nayfach, S. et al. Metagenomic compendium of 189,680 DNA viruses from the human gut microbiome. *Nat. Microbiol.* **6**, 960–970 (2021).
46. Athukoralage, J. S. et al. An anti-CRISPR viral ring nuclease subverts type III CRISPR immunity. *Nature* **577**, 572–575 (2020).
47. Bondy-Denomy, J., Pawluk, A., Maxwell, K. L. & Davidson, A. R. Bacteriophage genes that inactivate the CRISPR/Cas bacterial immune system. *Nature* **493**, 429–432 (2013).
48. Uribe, R. V. et al. Discovery and characterization of Cas9 inhibitors disseminated across seven bacterial phyla. *Cell Host Microbe* **25**, 233–241 (2019).
49. Manik, M. K. et al. Cyclic ADP ribose isomers: production, chemical structures, and immune signaling. *Science* **377**, eadc8969 (2022).
50. MacLean, R. C. & San Millan, A. The evolution of antibiotic resistance. *Science* **365**, 1082–1083 (2019).
51. Kortright, K. E., Chan, B. K., Koff, J. L. & Turner, P. E. Phage therapy: a renewed approach to combat antibiotic-resistant bacteria. *Cell Host Microbe* **25**, 219–232 (2019).
52. Nobrega, F. L., Costa, A. R., Kluskens, L. D. & Azeredo, J. Revisiting phage therapy: new applications for old resources. *Trends Microbiol.* **23**, 185–191 (2015).
53. Federici, S. et al. Targeted suppression of human IBD-associated gut microbiota commensals by phage consortia for treatment of intestinal inflammation. *Cell* **185**, 2879–2898 (2022).
54. Hussain, F. A. et al. Rapid evolutionary turnover of mobile genetic elements drives bacterial resistance to phages. *Science* **374**, 488–492 (2021).
55. LeGault, K. N. et al. Temporal shifts in antibiotic resistance elements govern phage-pathogen conflicts. *Science* **373**, eabg2166 (2021).
56. Gilchrist, C. L. M. & Chooi, Y.-H. clinker & clustermap.js: automatic generation of gene cluster comparison figures. *Bioinformatics* **37**, 2473–2475 (2021).

Methods

Bacterial strains and growth conditions

Bacteria were grown in magnesium manganese broth (MMB; LB + 0.1 mM $MnCl_2$ + 5 mM $MgCl_2$) at 37 °C shaking at 200 r.p.m., unless specified otherwise. To ensure the presence of an integrated antibiotics resistance cassette in the *B. subtilis* genome, the appropriate antibiotics were added at the following concentration: spectinomycin (100 μg ml^{-1}) or chloramphenicol (5 μg ml^{-1}). *E. coli* strain NEB 5-alpha (NEB catalogue number C2987H) was grown in LB. Whenever applicable, media were supplemented with ampicillin (100 μg ml^{-1}).

Defence systems used in this study were cloned previously[18] under their native promoter into the *amyE* locus of the *B. subtilis* BEST7003 genome. The source organisms of the specific systems used in this study are as follows: Thoeris (*B. cereus* MSX-D12), Hachiman (*B. cereus* B4087), Gabija (*B. cereus* VD045), Septu (*Bacillus thuringiensis* HD12) and Lamassu (*Bacillus* sp. NIO-1130).

Phage strains, isolation, cultivation and sequencing

The *B. subtilis* phages phi3T (Bacillus Genetic Stock Center (BGSC) ID 1L1, GenBank accession KY030782.1), SPβ (BGSC ID 1L5, GenBank accession AF020713.1), SPR (BGSC ID 1L56, GenBank accession OM236515.1) and SPO1 (BGSC ID 1P4, GenBank accession NC_011421.1) were obtained from the BGSC. Phages from the SBSphiJ group were isolated by us in previous studies[18,33]. Other phages used in this study were isolated by us from soil samples on *B. subtilis* BEST7003 culture as described previously[18]. For this, soil samples were added to *B. subtilis* BEST7003 culture and incubated overnight to enrich for *B. subtilis* phages. The enriched sample was centrifuged and filtered through 0.45-μm filters, and the filtered supernatant was used to carry out double-layer plaque assays as described previously[57]. Single plaques that appeared after overnight incubation at room temperature were picked, re-isolated three times, and amplified as described below.

Phages were propagated by picking a single phage plaque into a liquid culture of *B. subtilis* BEST7003 grown at 37 °C to an optical density at 600 nm (OD_{600nm}) of 0.3 in MMB broth until culture collapse (or 3 h in the case of no lysis). The culture was then centrifuged for 10 min at 3,200 *g* and the supernatant was filtered through a 0.45-μm filter to get rid of remaining bacteria and bacterial debris.

High-titre phage lysates (>10^7 PFUs ml^{-1}) were used for DNA extraction. A 500 μl volume of the phage lysate was treated with DNase-I (Merck catalogue number 11284932001) added to a final concentration of 20 mg ml^{-1} and incubated at 37 °C for 1 h to remove bacterial DNA. DNA was extracted using the QIAGEN DNeasy blood and tissue kit (catalogue number 69504) starting from the Proteinase-K treatment step.

Phages from the SBSphiJ and SPβ groups were sequenced using a modified Nextera protocol as previously described[58]. Following Illumina sequencing, adapter sequences were removed from the reads using Cutadapt v2.8 (ref. 59) with the option -q 5. The trimmed reads from each phage genome were assembled into scaffolds using SPAdes genome assembler v3.14.0 (ref. 60), using the –careful flag.

The genomes of phages from the SPO1 group were sequenced using a long-read PacBio method, owing to the high amount of modified bases in these phages. For library construction of phages from the SPO1 group, 1 μg of genomic DNA samples was fragmented using g-tubes (Covaris). Sheared DNA was purified with AMPure PB beads and was used to construct a SMRTbell library according to the PacBio library construction guidelines[61]. Samples were barcoded using Barcoded Overhang Adapters and pooled to one final library. The quantity and quality of the SMRTbell library were determined using the Qubit HS DNA kit and Agilent TapeStation Genomic DNA. No size selection was carried out. The PacBio sequencing primer was then annealed to the SMRTbell library followed by binding of the polymerase to the primer–library complex. The library was loaded onto one SMRT cell in the PacBio Sequel system and sequenced in continuous long-read mode for 10 h.

All phage genomes sequenced and assembled in this study were analysed with Prodigal v2.6.3 (ref. 62; default parameters) to predict ORFs.

Plaque assays

Phage titre was determined using the small drop plaque assay method[63]. A 400 μl volume of overnight culture of bacteria was mixed with 0.5% agar and 30 ml MMB and poured into a 10-cm square plate followed by incubation for 1 h at room temperature. In cases of bacteria expressing anti-defence candidates and in the experiment with the phage SBSphiJ with a *tad2* knock-in, 1 mM IPTG was added to the 30 ml MMB 0.5% agar. In cases of bacteria expressing dCas9–gRNA constructs, 0.002% xylose was added to the medium. Tenfold serial dilutions in MMB were carried out for each of the tested phages and 10-μl drops were put on the bacterial layer. After the drops had dried up, the plates were inverted and incubated at room temperature overnight. PFUs were determined by counting the derived plaques after overnight incubation and lysate titre was determined by calculating PFUs per millilitre. When no individual plaques could be identified, a faint lysis zone across the drop area was considered to be 10 plaques. The efficiency of plating was measured by comparing plaque assay results for control bacteria and those for bacteria containing the defence system and/or a candidate anti-defence gene.

Prediction of candidate anti-defence genes

Predicted protein sequences from all phage genomes in each phage family were clustered into groups of homologues using the cluster module in MMSeqs2 release 12-113e3 (ref. 64), with the parameters -e 10, -c 0.8, -s 8, --min-seq-id 0.3 and the flag --single-step-clustering. For each defence system, anti-defence candidates were defined as clusters that have a representation in all of the phages that overcome the defence system and are absent from all of the phages that are blocked by the defence system. One member was chosen from each cluster as a candidate anti-defence gene for further experimental testing (Supplementary Table 7). In the case of the Hachiman defence system, only predicted genes with no known function were tested experimentally. *gad2* was predicted on the basis of its localization in the sane locus as *gad1* in the phages SPβL6 and SPβL7.

Cloning of candidate anti-defence genes

The DNA of each anti-defence candidate was amplified from the source phage genome using KAPA HiFi HotStart ReadyMix (Roche catalogue number KK2601) and primers provided in Supplementary Table 7, and cloned using the NEBuilder HiFI DNA Assembly cloning kit (NEB, no. E5520S) into the pSG-thrC-Phspank vector. Homologues of verified anti-defence genes (Supplementary Tables 8, 10, 12 and 17) were synthesized and cloned by Genscript Corp. The anti-defence candidates were cloned into the pSG-thrC-Phspank vector[33] and transformed into NEB 5-alpha competent cells. The cloned vector was subsequently transformed into *B. subtilis* BEST7003 cells containing the respective defence system integrated into the *amyE* locus[18], resulting in cultures expressing both a defence system and the corresponding anti-defence gene candidate, integrated into the *amyE* and *thrC* loci, respectively. As a negative control, a transformant with an identical plasmid containing sfGFP instead of the anti-defence gene was used. Transformation to *B. subtilis* was carried out using MC medium as previously described[18] and transformants were plated on LB agar plates supplemented with 5 μg ml^{-1} chloramphenicol and incubated overnight at 30 °C. Whole-genome sequencing was then applied to all transformed *B. subtilis* strains, and Breseq (v0.34.1) analysis[65] was used to verify the integrity of the inserts and lack of mutations.

gad1 knockout in phi3T lysogenic strain

The upstream and downstream homologous arms of *gad1* were amplified from the phi3T phage genome using the PCR primer pairs Gad1_AF and Gad1_AR, and Gad1_BF and Gad1_BR, respectively (Supplementary

Table 15). The spectinomycin resistance gene cassette was amplified from the vector pJmp3 (Addgene plasmid number 79875) using the PCR primers Spec_F and Spec_R (Supplementary Table 15). The pJmp3 backbone was amplified using the primers Vector_F and Vector_R (Supplementary Table 15).

These three parts were assembled together with the pJmp3 backbone using the NEBuilder HiFi DNA Assembly cloning kit (NEB catalogue number E5520S) and transformed into *E. coli* NEB 5-alpha competent cells. The cloned vector was then transformed into the phi3T lysogenic strain (BGSC ID 1L1) using MC medium[18] and was plated on LB agar plates supplemented with 100 μg ml^{-1} spectinomycin and incubated overnight at 30 °C. The modified phi3T prophage was induced from the lysogenic bacterial strain grown to an OD_{600nm} of 0.3 by the addition of 0.5 μg ml^{-1} mitomycin C (Sigma, M0503). After 3 h, the culture was centrifuged for 10 min at 3,200*g* and the supernatant containing the modified phages was collected and filtered through 0.2-μm filters. Whole-genome sequencing was carried out to verify the sequence of the modified phage.

gad2 knockout in SPβL7 using Cas13a

Cas13a was amplified from the pBA559 plasmid[66] with the primers cas13a_fwd and cas13a_rev. The xylose promoter and homology arms for integration into the *thrC* site were amplified from the plasmid pJG_thrC_dCAS9_gRNA[33] with the primers dcas9xylProm_fwd and dcas9xylProm_rev. The gRNA complementary to the beginning of *gad2* was amplified from the pBA559 plasmid with the primers gRNAcas13_fwd and gRNAcas13L7159_rev. Plasmid assembly was conducted using the NEBuilder HiFi DNA Assembly cloning kit (NEB, catalogue number E5520S) and the cloned vector was transformed into NEB 5-alpha competent cells. The cloned vector was subsequently transformed into the *thrC* site of *B. subtilis* BEST7003.

For the selection of *gad2*-knockout SPβL7 phages, an overnight culture of the Cas13a-gRNA-containing bacteria was diluted 1:100 with MMB agar 0.5% with 0.2% xylose, and grown for 1 h at room temperature. Then, 10^8 PFUs of the phage SPβL7 were spread on the plate. The next day, several individual plaques were collected and propagated with 1 ml of the Cas13a-gRNA-containing bacteria. *gad2* knockout was verified using PCR primers L7159Fchk and L7159Rchk. Sequencing of the product demonstrated deletion of bases 109,505–110,753 from the SPβL7 genome, spanning the entire *gad2* gene and the *gad2* promoter. The selected knockout phage was purified three times on *B. subtilis* BEST7003.

Gabija and Gabija + Gad1 complex assembly and in vitro nuclease activity

bcGajAB and bcGajAB + *Shewanella* sp. phage 1/4 Gad1 complexes were purified as described elsewhere[41]. A 56-base-pair double-stranded DNA (dsDNA) with a sequence-specific motif derived from the phage lambda (5′-TTTTTTTTTTTTTTTTTAATAACCCGGTTATTTTTTTTTTTTTTTTTTTTTTT-3′)[39] was pre-incubated with purified GajAB or GajAB + Gad1 in 20 μl DNA cleavage reactions containing 1 μM dsDNA, 1 μM GajAB or GajAB + Gad1, 1 mM $MgCl_2$, 20 mM Tris-HCl pH 9.0 for 1, 5, 10, 15 and 20 min at 37 °C. Following incubation, reactions were stopped with DNA loading buffer containing EDTA and 10 μl was analysed on a 2% Tris–borate (TB) agarose gel. Gels were run at 250 V for 40 min at 4 °C, and then stained by rocking at room temperature in TB buffer with 10 μg ml^{-1} ethidium bromide for 30 min. Gels were destained in TB buffer for 40 min and imaged with a ChemiDoc MP Imaging System.

Gad2 pulldown assay

The GajA, GajB and Gad1 proteins were co-expressed together using a custom pET vector with an N-terminal 6×His–SUMO2–5×GS tag on GajA and a ribosome-binding site between GajA and GajB, and between GajB and Gad1. *B. laterosporus* Gad2 was cloned from synthetic DNA (Integrated DNA Technologies) into a custom pBAD vector containing a chloramphenicol resistance gene and an IPTG-inducible promoter or a custom pET vector with an N-terminal 6×His–SUMO2 tag. Plasmids were transformed and expressed in BL21(DE3) or LOBSTR-BL21(DE3)-RIL (Kerafast) cells and subjected to Ni-NTA column chromatography and SUMO2 cleavage with SENP2. Gad2 pulldown was analysed by SDS–PAGE and Coomassie blue staining.

GajAB DNA–Gad2 cleavage assay

GajAB complex was expressed and purified as previously described[41]. Briefly, Gad2 was expressed with an N-terminal 6×His–SUMO2 tag in LOBSTR-BL21(DE3)-RIL cells (Kerafast) and purified using Ni-NTA resin (Qiagen) followed by size-exclusion chromatography (SEC) using a 16/600 Superdex 200 column (Cytiva). The same 56-bp dsDNA substrate as used in GajAB DNA cleavage assays was incubated with 1 μM, 4 μM or 8 μM Gad2 in a 20 μl DNA cleavage reaction containing 0.5 μM NAD^+ (Sigma Aldrich), 0.5 μM NTPs, 1 μM dsDNA, 1 mM $MgCl_2$, 20 mM Tris-HCl pH 9.0 for 10 min on ice. A 1 μM concentration of GajAB was added to the reaction and incubated for 20 min at 37 °C. A control Gad2-alone lane was run to demonstrate slight nucleic acid contamination within the Gad2 protein preparation. Following incubation, reactions were terminated with DNA loading buffer containing 60 mM EDTA and 10 μl was analysed on a 2% TB agarose gel run at 250 V for 30 min. The gel was post-stained by rocking at room temperature with TB buffer containing 10 μg ml^{-1} ethidium bromide, destained in TB buffer alone for 30 min and imaged on a ChemiDoc MP Imaging System.

Construction of dCas9 and gRNA cassettes for integration in *B. subtilis thrC* site

The plasmid pJG_thrC_dCAS9_gRNA was constructed as previously described[33]. To insert new spacers, two fragments were amplified from pJG_thrC_dCAS9_gRNA and the new spacer was introduced into the overlap of primers designed for NEBuilder HiFi DNA Assembly (NEB, number E5520S). For the gRNA used to target *tad2*, the first fragment was amplified using the primers JG528 and JG525, and the second using the primers JG529 and JG524 (Supplementary Table 15). The resulting assembled construct had the gRNA sequence aagatgatgttcccaaacac. For the gRNA used to target *had1*, the first fragment was amplified using the primers JG389 and JG381, and the second using the primers JG390 and JG382 (Supplementary Table 15). The resulting assembled construct had the gRNA sequence gcttgctaggattagtgtcc. The gRNA sequence ctatgattgatttttttagc was used as a control. It was constructed as mentioned above, with the primers JG389 and JG378, and JG390 and JG388 (Supplementary Table 15). Shuttle vectors were propagated in *E. coli* NEB 5-alpha with 100 μg ml^{-1} ampicillin selection. Plasmids were isolated from *E. coli* NEB 5-alpha before transformation into the appropriate *B. subtilis* BEST7003 strains. The vectors containing the dCas9–gRNA sequences were cloned into *B. subtilis* strains containing the respective defence system, as well as into a control strain lacking the defence system.

Knock-in of *had1* and *tad2* into phage SBSphiJ and Gad1 into phage SPβ

The DNA sequence of *tad2*, together with the Phspank promoter, was amplified from the Tad2-containing pSG-thrC-Phspank plasmid using KAPA HiFi HotStart ReadyMix (Roche, catalogue number KK2601) with the primer pair tad2KIF and tad2KIr (Supplementary Table 15). The DNA sequence of *had1*, together with its upstream intergenic region, was amplified from the genome of the phage SBSphiJ4 with the primer pair had1KIF and had1KIR (Supplementary Table 15). The backbone fragment with the upstream and downstream genomic arms (±1.2 kb) for the integration site of *tad2* and *had1* was amplified from the plasmid used previously for knock-in of the *tad1* gene[33], with the primer pair backboneKIF and backboneKIR (Supplementary Table 15). The DNA sequence of *gad1*, together with its upstream intergenic region,

was amplified from the genome of the phage phi3T with the primer pair gad1KIF and gad1KIR (Supplementary Table 15). The upstream and downstream genomic arms (±1.2 kb) for the integration site of the *gad1* gene within the SPβ genome were amplified from the genome of the phage SPβ using the primer pair gad1LFF and gad1LFR, and the primer pair gad1RFF and gad1LRR (Supplementary Table 15). Cloning was carried out using the NEBuilder HiFi DNA Assembly cloning kit (NEB, number E5520S) and the cloned vector was transformed into NEB 5-alpha competent cells. The cloned vector was subsequently transformed into the *thrC* site of *B. subtilis* BEST7003.

The *tad2*-, *had1*- and *gad1*-containing *B. subtilis* BEST7003 strains were then infected with the phages SBSphiJ (*tad2* and *had1*) or SPβ (*gad1*) with a multiplicity of infection (MOI) of 0.1 and cell lysates were collected. Tad2 lysate was used to infect a Thoeris-containing *B. subtilis* culture in two consecutive rounds with an MOI of 2 in each round (30 °C, 1 mM IPTG). Had1 lysate was used to infect a Hachiman-containing *B. subtilis* culture in two consecutive rounds with an MOI of 2 in each round (25 °C). Gad1 lysate was used to infect a Gabija-containing *B. subtilis* culture in two consecutive rounds with an MOI of 2 in each round (25 °C). Several plaques were collected and screened using PCR for the desired insertion within the phage genome. Phages with anti-defence genes were purified three times on *B. subtilis* BEST7003. Purified phages were verified again for the presence of *tad2*, *had1* and *gad1* using PCR amplifications.

Identification of anti-defence homologues and phylogenetic reconstruction

Homologues of anti-defence genes were searched in the Metagenomic Gut Virus (MGV)[45] database using the "search" option of MMseqs release 12-113e3 with default parameters. Homologues of Gad1, Gad2 and Had1 were searched in the Integrated Microbial Genomes (IMG) database[44] using the blast option in the IMG web server. Gad1 and Gad2 homologues were searched using the default parameters, whereas Had1 homologues were searched using an e-value of 10 owing to their short size. For Gad1 and Had1, this process was repeated iteratively for homologues that were found, until convergence. For Tad2, owing to the multitude of homologues, homology search was carried out using the "search" option of MMseqs release 12-113e3 with default parameters, against about 38,000 prokaryotic genomes downloaded from the IMG database in October 2017.

For each family of anti-defence proteins, the unique (non-redundant) sequences were used for multiple sequence alignment with MAFFT v7.402 (ref. 67) using default parameters. Phylogenetic trees were constructed using IQ-TREE v1.6.5 (ref. 68) with the -m LG parameter. The online tool iTOL24 (v5)[69] was used for tree visualization. Phage family annotations were based on the prediction in the MGV database. The host phyla annotations were based on either the prediction in the MGV database, or the IMG taxonomy of the bacteria in which the prophage was found. Gabija and Thoeris defence systems were found in the bacterial genomes using DefenseFinder[38] v1.0.9 and database release 1.2.3.

Preparation of filtered cell lysates

For generating filtered cell lysates, we used *B. subtilis* BEST7003 cells co-expressing Tad2 and the *B. cereus* MSX-D12 Thoeris system in which ThsA was inactivated (ThsB + $ThsA_{N112A}$). Tad2 was integrated in the *thrC* locus as described above and expressed from an inducible Phspank promoter, and the Thoeris system was integrated in the *amyE* locus and expressed from its native promoter as described above. Controls included cells expressing only the ThsB + ThsA(N112A) Thoeris system without Tad2, as well as cells lacking both the Thoeris system and Tad2. These cultures were grown overnight and then diluted 1:100 in 250 ml MMB medium supplemented with 1 mM IPTG and grown at 37 °C, 200 r.p.m. shaking for 120 min followed by incubation and shaking at 25 °C, 200 r.p.m. until reaching an OD_{600nm} of 0.3. At this point, a sample of 40 ml was taken as the uninfected (time 0 min) sample, and the SBSphiJ phage was added to the remaining 210-ml culture at an MOI of 10. Flasks were incubated at 25 °C with shaking (200 r.p.m.), for the duration of the experiment. Samples of 40 ml were collected at time points 75, 90 and 105 min post-infection. Immediately after sample removal (including time point 0 min), the 40-ml sample tubes were centrifuged at 4 °C for 10 min at 3,200*g* to pellet the cells. The supernatant was discarded, and the pellet was flash frozen and stored at −80 °C.

To extract cell metabolites from frozen pellets, 600 µl of 100 mM Na phosphate buffer (pH 8.0) was added to each pellet. Samples were transferred to FastPrep Lysing Matrix B in a 2-ml tube (MP Biomedicals, number 116911100) and lysed at 4 °C using a FastPrep bead beater for 2 × 40 s at 6 m s^{-1}. Tubes were then centrifuged at 4 °C for 10 min at 15,000*g*. The supernatant was then transferred to an Amicon Ultra-0.5 Centrifugal Filter Unit 3 kDa (Merck Millipore, no. UFC500396) and centrifuged for 45 min at 4 °C, 12,000*g*. Filtered lysates were taken for in vitro ThsA-based NADase activity assay.

Expression and purification of ThsA

B. cereus MSX-D12 *thsA* fused to a C-terminal Twin-Strep tag was cloned into a pACYC-Duet1 plasmid (Addgene plasmid number 71147). The protein was expressed under the control of the T7 promoter together with a C-terminal Twin-Strep tag for subsequent purification. Expression was carried out in 5 l LB medium supplemented with chloramphenicol (34 mg ml^{-1}) in *E. coli* BL21(DE3) cells. Induction was carried out with 0.2 mM IPTG at 15 °C overnight. The cultures were collected by centrifugation and lysed by a cooled cell disrupter (Constant Systems) in 100 ml lysis buffer composed of 20 mM HEPES pH 7.5, 0.3 M NaCl, 10% glycerol, 5 mM β-mercaptoethanol, 200,000 U 100 ml^{-1} lysozyme, 20 µg ml^{-1} DNase, 1 mM $MgCl_2$, 1 mM phenylmethylsulfonyl fluoride and protease inhibitor cocktail (Millipore, 539134). Cell debris was sedimented by centrifugation, and the lysate supernatant was incubated with 2 ml washed StrepTactin XT beads (IBA, 2-5030–025) for 1 h at 4 °C. The sedimented beads were then packed into a column connected to an fast protein liquid chromatography allowing the lysate to pass through the column at 1 ml min^{-1}. The column was washed with 20 ml lysis buffer. ThsA was eluted from the column using elution buffer containing 50 mM biotin, 100 mM Tris pH 8, 150 mM NaCl and 1 mM EDTA. Peaks containing the ThsA protein were injected into a SEC column (Superdex 200_16/60, GE Healthcare, 28-9893-35) equilibrated with SEC buffer (20 mM HEPES pH 7.5, 200 mM NaCl and 2 mM dithiothreitol (DTT)). Peaks were collected from the SEC column, aliquoted and frozen at −80 °C to be used for subsequent experiments.

ThsA-based NADase activity assay

NADase reaction was carried out in black 96-well half-area plates (Corning, 3694). In each reaction microwell, purified ThsA protein was added to cell lysate, to in vitro reactions of Tad2 with 1″–3′ gcADPR, or to 100 mM sodium phosphate buffer pH 8.0. A 5 µl volume of 5 mM nicotinamide 1,N^6-ethenoadenine dinucleotide (εNAD$^+$, Sigma, N2630) solution was added to each well immediately before the beginning of measurements, resulting in a final concentration of 100 nM ThsA protein in a 50 µl final volume reaction. Plates were incubated inside a Tecan Infinite M200 plate reader at 25 °C, and measurements were taken at 300 nm excitation wavelength and 410 nm emission wavelength. The reaction rate was calculated from the linear part of the initial reaction.

Tad2 protein cloning, expression and purification for biochemistry

The SPO1 *tad2* gene was cloned into the expression vector pET28-bdSumo as described previously[33]. Tad2 was expressed in *E. coli* BL21(DE3) by induction with 200 µM IPTG at 15 °C overnight. A 2-l culture of bacteria expressing Tad2 was collected and lysed by a cooled cell disrupter (Constant Systems) in lysis buffer (50 mM Tris pH 8, 0.25 M NaCl, 10% glycerol) containing 200,000 U 100 ml^{-1} lysozyme, 20 µg ml^{-1} DNase, 1 mM $MgCl_2$, 1 mM phenylmethylsulfonyl fluoride and protease

inhibitor cocktail. After clarification of the supernatant by centrifugation, the lysate was incubated with 5 ml washed Ni beads (Adar Biotech) for 1 h at 4 °C. After removing the supernatant, the beads were washed four times with 50 ml lysis buffer. Tad2 was eluted by incubation of the beads with 10 ml cleavage buffer (50 mM Tris pH 8, 0.25 M NaCl, 10% glycerol and 0.4 mg bdSumo protease) for 1 h at 23 °C. The supernatant, containing cleaved Tad2, was removed, and an additional 5 ml cleavage buffer was added to the beads and left overnight at 4 °C. The two elution solutions were combined, concentrated and applied to a SEC column (HiLoad_16/60_Superdex75 prep-grade, Cytiva) equilibrated with 50 mM Tris pH 8, 100 mM NaCl. Pure Tad2 migrating as a single peak was pooled and flash frozen in aliquots using liquid nitrogen and stored at −80 °C.

Incubation of purified 1″–3′ gcADPR with Tad2

A 2.4 μM concentration of purified Tad2 was incubated with 600 nM of 1″–3′ gcADPR in 100 mM Na phosphate buffer, pH 8.0 for 10 min, at 25 °C, followed by an additional 10-min incubation at either 95 °C or 25 °C. Following incubation, samples were left on ice for 1 min. The samples were then used for ThsA-based NADase activity assays as described above.

Analytical SEC analysis of apo and ligand-bound Tad2

A 50-μl volume of Tad2 (158 μM) was incubated with 30 μl of 1 mM 1″–3′ gcADPR at 25 °C, in 0.1 M NaCl, 50 mM Tris-HCl pH 8.0, for 20 min. The incubated mixture, and an apo protein incubated with an identical buffer without the ligand, were then loaded on an SEC Superdex_200_10/300 analytical column (PBS buffer) and monitored for absorption at both 260 nm and 280 nm. The oligomeric nature of the Tad2 apo protein was evaluated by comparing the retention time of apo Tad2 to that of five internal standard proteins (ribonuclease 13.7 kDa, chymotrypsin 25 kDa, BSA 66 kDa, Aldolase 160 kDa and apoferritin 443 kDa) using an SEC Superdex_200_10/300.

Surface plasmon resonance measurements of Tad2 binding to 1″–3′ gcADPR and cADPR

Binding of 1″–3′ gcADPR to Tad2 was monitored by surface plasmon resonance with a BIAcore S200 apparatus (Cytiva). Tad2 was immobilized on a CM5 S Series chip (Cytiva) by amine coupling chemistry using the following protocol: chip activation was carried out with a freshly prepared mixture of *N*-hydroxysuccinimide (50 mM in water) and 1-ethyl-3-(3-dimethylaminopropyl) carbodiimide (195 mM in water) for 7.5 min in DPBS (Sartorius, SKU 02-023-5 A; flow rate of 10 μl min^{-1}). DPBS served as the running buffer along the experiment. The Tad2 protein (5 μg ml^{-1} in 150 mM sodium acetate buffer, pH 3.8) was injected for 5 min (flow rate 10 μl min^{-1}) and the remaining activated carboxylic groups were blocked by injection of 1 M ethanolamine hydrochloride, pH 8.0, for 5 min (flow rate 10 μl min^{-1}). Subsequently, a total of 1,800 response units of Tad2 were immobilized onto the chip. Before data collection, a normalization cycle and then a priming cycle were run to stabilize the instrument. Binding of 1″–3′ gcADPR to Tad2 was monitored by injecting 1″–3′ gcADPR at multiple concentrations for 2 min at 25 °C and a flow rate of 50 μl min^{-1}. Dissociation was carried out for 180 s. No regeneration step was required after ligand binding as the dissociation reached baseline spontaneously. Sensorgrams were fitted to a 1:1 binding model (S200 evaluation software 1.1) that yielded the kinetic constants (association constant (k_a) and k_d) of the interaction. k_d divided by k_a yields the steady-state K_D. cADPR, which served as a control, did not bind, as expected.

Protein cloning, expression and purification

Synthetic DNA fragments (Integrated DNA Technologies) of cmTad1, $AbTIR^{TIR}$ (Δ1–156), cbTad1, SPO1 Tad2 and *B. toyonensis* Had1 genes were cloned into a custom pET expression vector containing an N-terminal 6×His–SUMO2 tag and an ampicillin resistance gene by Gibson assembly, as previously described[70]. Three colonies of BL21(DE3) RIL *E. coli* transformed with these plasmids and grown on MDG agar plates (1.5% agar, 2 mM $MgSO_4$, 0.5% glucose, 25 mM Na_2HPO_4, 25 mM KH_2PO_4, 50 mM NH_4Cl, 5 mM Na_2SO_4, 0.25% aspartic acid, 2–50 μM trace metals) were picked into a 30-ml MDG starter culture and shaken overnight at 230 r.p.m. and 37 °C. A 1-l culture of M9ZB expression medium (2 mM $MgSO_4$, 0.5% glycerol, 47.8 mM Na_2HPO_4, 22 mM KH_2PO_4, 18.7 mM NH_4Cl, 85.6 mM NaCl, 1% Cas-amino acids, 2–50 μM trace metals, 100 μg ml^{-1} ampicillin and 34 μg ml^{-1} chloramphenicol) was seeded with 15-ml starter culture and grown at 230 r.p.m. and 37 °C to an OD_{600} of 2 before induction of expression with 0.5 mM IPTG and incubation at 230 r.p.m. and 16 °C for 16 h. For $AbTIR^{TIR}$ expression, nicotinamide-supplemented 2YT expression medium (1.6% w/v tryptone, 1% w/v yeast extract, 342 mM NaCl, 10 mM NAM, 100 μg ml^{-1} ampicillin, 34 μg ml^{-1} chloramphenicol) was used instead. Cells were collected by centrifugation, resuspended in lysis buffer (20 mM HEPES-KOH pH 7.5, 400 mM NaCl, 30 mM imidazole, 10% glycerol, 1 mM DTT), lysed by sonication and clarified by centrifugation at 25,000 *g* for 20 min. Lysate was passed over 8 ml Ni-NTA resin (Qiagen), washed with 70 ml wash buffer (20 mM HEPES-KOH pH 7.5, 1 M NaCl, 30 mM imidazole, 10% glycerol, 1 mM DTT), eluted with lysis buffer supplemented to 300 mM imidazole, and dialysed in 14-kDa dialysis tubing in dialysis buffer (20 mM HEPES-KOH pH 7.5, 250 mM KCl, 1 mM DTT) overnight at 4 °C with purified human SENP2 for 6×His–SUMO2 tag cleavage. For crystallography, proteins were further purified on a Superdex 75 16/600 SEC column (Cytiva). Final samples were concentrated to >20 mg ml^{-1}, flash frozen, and stored at −80 °C.

ThsB′ was cloned and purified similarly as described above, except that it was cloned into a custom pET vector containing a C-terminal 6× His tag and a chloramphenicol resistance gene, transformed into BL21(DE3) cells, grown in the presence of chloramphenicol alone, expressed in 2YT medium with 10 mM NAM, and concentrated to 4 mg ml^{-1} after dialysis before flash-freezing and storage.

1″–2′ gcADPR and 1″–3′ gcADPR production and purification

gcADPR molecules were produced as described previously[33]. For 1″–2′ gcADPR production, purified $AbTIR^{TIR}$, a bacterial enzyme that efficiently converts NAD^+ to 1″–2′ gcADPR[49], was used to set up 300-μl reactions (50 mM HEPES-KOH, 150 mM NaCl, 20 mM NAD^+, 40 μM $AbTIR^{TIR}$). For 1″–3′ gcADPR production, purified ThsB′[33] was used to set up 50-ml reactions (50 mM HEPES-KOH pH 7.5, 150 mM NaCl, 2 mM NAD^+, 16 μM ThsB′). Reactions were carried out at room temperature for 24–48 h before boiling at 95 °C for 10 min, pelleting at 13,500 *g* for 20 min, and filtering through a 10-kDa MWCO filter (Amicon). For the $AbTIR^{TIR}$ reaction, filtrate was diluted to 30 ml with PBS followed by addition of 200 μM purified cmTad1. For the ThsB′ reaction, 10 μM purified cmTad1 was added directly to 50 ml of filtrate. Mixtures were then incubated for 1 h at room temperature to allow cmTad1–gcADPR complex formation. The complexes were washed by successive concentration and dilution in a 10-kDa MWCO filter first with five 1:20 dilutions in PBS followed by five 1:20 washes in water. Complexes were concentrated to >3 mM before final release and extraction of gcADPR by boiling at 95 °C for 10 min, pelleting at 13,500 *g* for 20 min, filtering through a 3 kDa MWCO filter, and collecting the filtrate. Final purity and concentration were assessed by HPLC.

Protein crystallization and structural analysis

cbTad1, SPO1 Tad2 and Had1 crystals were grown by the hanging-drop method in EasyXtal 15-well trays (NeXtal) at 16 °C. Hanging drops were set using 1 μl of diluted protein solution (5–10 mg ml^{-1} protein, 20 mM HEPES-KOH pH 7.5, 70–80 mM KCl, 1 mM TCEP) and 1 μl reservoir solution over a 400 μl well of reservoir solution. Proteins were crystallized and cryoprotected under the following conditions before being collected by flash-freezing in liquid nitrogen. For cbTad1 complexed with 1″–3′ gcADPR, crystals were grown for 3 weeks in drops supplemented

with 500 μM ThsB′-derived 1″–3′ gcADPR using reservoir solution containing 0.2 M $MgCl_2$, 0.1 M Tris-HCl pH 8.5 and 3.4 M 1,6-hexanediol. For SPO1 Tad2 in the apo state, crystals were grown for 1 week using reservoir solution containing 0.1 M 2-(*N*-morpholino) ethanesulfonic acid pH 6.5, 10% (v/v) 1,4-dioxane and 1.6 M ammonium sulfate before being cryoprotected with reservoir solution supplemented with 25% (v/v) glycerol. For SPO1 Tad2 complexed with 1″–3′ gcADPR, crystals were grown for 1 week in drops supplemented with 500 μM ThsB′-derived 1″–3′ gcADPR using reservoir solution containing 0.2 M magnesium nitrate and 18% (w/v) PEG 3350 before being cryoprotected with reservoir solution supplemented with 20% (v/v) ethylene glycol and 1 mM 1″–3′ gcADPR. For SPO1 Tad2 complexed with 1″–2′ gcADPR, crystals were grown for 1 week in drops supplemented with 500 μM $AbTIR^{TIR}$-derived 1″–2′ gcADPR using reservoir solution containing 0.1 M Tris-HCl pH 8.5, 12% (v/v) glycerol and 1.5 M ammonium sulfate before being cryoprotected with reservoir solution supplemented with 15% (v/v) ethylene glycol and 1 mM 1″–2′ gcADPR. For Had1 in the apo state, crystals were grown for 1 week using reservoir solution containing 100 mM MES pH 6.2 and 30% PEG 4000 before being cryoprotected with reservoir solution supplemented with 10% (v/v) ethylene glycol.

cbTad1 and SPO1 Tad2 X-ray diffraction data were collected at the Advanced Photon Source (beamline 24-ID-C), and data were processed with XDS[71] and Aimless[72] using the SSRL autoxds script (A. Gonzalez, Stanford SSRL). Phases were determined by molecular replacement in Phenix using either previously determined cbTad1 structures[33] (Protein Data Bank 7UAV and 7UAW) or sequence-predicted SPO1 Tad2 truncated structures from ColabFold v1.5.2 (ref. 73). Model building was carried out in Coot[74]; refinement was carried out in Phenix[75]. Had1 X-ray diffraction data were collected at the Advanced Light Source (beamline 8.2.1) and data were processed with XDS[71] and Aimless[72] using the SSRL autoxds script (A. Gonzalez, Stanford, SSRL). Experimental phase information was determined by molecular replacement using a dimeric Had1 AlphaFold2-predicted structure[73] in Phenix[75]. Model building was completed in Coot[74] and then refined in Phenix[75]. Statistics were analysed as presented in Extended Data Table 1 and refs. 76–78, and structure figures were produced in PyMOL. Final structures were refined to stereochemistry statistics for Ramachandran plot (favoured/allowed), rotamer outliers and MolProbity scores as follows: cbTad1–1″–3′-gcADPR, 95.88/4.12%, 0.92%, 1.47; SPO1 Tad2 apo, 96.15/2.56%, 0.74%, 1.59; SPO1 Tad2–1″–3′-gcADPR, 99.18/0.82%, 1.5%, 1.33; SPO1 Tad2–1″–2′-gcADPR, 99.36/0.64%, 2.19%, 1.27; Had1, 96.18/3.82%, 0.69%, 1.20.

HPLC analysis of Tad2 incubation with 1″–3′ gcADPR

Reactions to analyse cleavage of 1″–3′ gcADPR were carried out in 120-μl reactions consisting of 50 mM Tris-HCl pH 7.5, 100 mM KCl, 5 mM $MgCl_2$, 1 mM $MnCl_2$, 50 μM gcADPR isomer, and either buffer or 1 μM Tad2. As a control, 1″–3′ gcADPR was also incubated with 1 μl Cap-Clip acid pyrophosphatase (known to cleave diphosphate linkages on mRNA caps; Fisher Scientific), using the manufacturer's recommended reaction conditions. Reactions were incubated at 37 °C for 1 h before filtration using a 3-kDa MWCO filter. Filtered reactions were analysed using a C18 column (Agilent Zorbax Bonus-RP 4.6 × 150 mm) heated to 40 °C and run at 1 ml min^{-1} using a buffer of 50 mM NaH_2PO_4-NaOH pH 6.8 supplemented with 3% acetonitrile.

Reporting summary

Further information on research design is available in the Nature Portfolio Reporting Summary linked to this article.

Data availability

Data that support the findings of this study are available in the article and Supplementary Tables 1–15. IMG and MGV accession numbers, protein sequences and nucleotide sequences are available in Supplementary Tables 8–14. Coordinates and structure factors for cbTad1–1″–3′-gcADPR, SPO1 Tad2 apo, SPO1 Tad2–1″–3′-gcADPR, SPO1 Tad2–1″–2′-gcADPR and Had1 have been deposited in the Protein Data Bank under the accession codes 8SMD, 8SME, 8SMF, 8SMG and 8TTO, respectively. The genome sequences of the phages SPO1L1–SPO1L5 and SPβL1–SPβL8 have been deposited with GenBank under accession codes OQ921336–OQ921348, respectively. Source data are provided with this paper.

57. Kropinski, A. M., Mazzocco, A., Waddell, T. E., Lingohr, E. & Johnson, R. P. in *Bacteriophages: Methods and Protocols* Vol. 1 (eds Kropinski, A. M. & Cloike, M. R. J.) 69–76 (Humana, 2009).
58. Baym, M. et al. Inexpensive multiplexed library preparation for megabase-sized genomes. *PLoS ONE* **10**, e0128036 (2011).
59. Martin, M. Cutadapt removes adapter sequences from high-throughput sequencing reads. *EMBnet.journal* **17**, 10 (2011).
60. Nurk, S. et al. Assembling genomes and mini-metagenomes from highly chimeric reads. *Res. Comput. Mol. Biol.* **7821**, 158–170 (2013).
61. *Procedure & Checklist – Preparing Multiplexed Microbial Libraries Using SMRTbell Express Template Prep Kit 2.0* (PacBio), version 8 https://www.pacb.com/wp-content/uploads/Procedure-Checklist---Preparing-Multiplexed-Microbial-Libraries-Using-SMRTbell-Express-Template-Prep-Kit-2.0.pdf (2021).
62. Hyatt, D. et al. Prodigal: prokaryotic gene recognition and translation initiation site identification. *BMC Bioinform.* **11**, 119 (2010).
63. Mazzocco, A., Waddell, T. E., Lingohr, E. & Johnson, R. P. in *Bacteriophages: Methods and Protocols* Vol. 1 (eds Kropinski, A. M. & Cloike, M. R. J.) 81–85 (Humana, 2009).
64. Steinegger, M. & Söding, J. MMseqs2 enables sensitive protein sequence searching for the analysis of massive data sets. *Nat. Biotechnol.* **35**, 1026–1028 (2017).
65. Deatherage, D. E. & Barrick, J. E. in *Engineering and Analyzing Multicellular Systems* (eds Sun, L. & Shou, W.) 165–188 (Humana, 2014).
66. Adler, B. A. et al. Broad-spectrum CRISPR-Cas13a enables efficient phage genome editing. *Nat. Microbiol.* **7**, 1967–1979 (2022).
67. Katoh, K. & Standley, D. M. MAFFT multiple sequence alignment software version 7: improvements in performance and usability. *Mol. Biol. Evol.* **30**, 772–780 (2013).
68. Nguyen, L.-T., Schmidt, H. A., von Haeseler, A. & Minh, B. Q. IQ-TREE: a fast and effective stochastic algorithm for estimating maximum-likelihood phylogenies. *Mol. Biol. Evol.* **32**, 268–274 (2015).
69. Letunic, I. & Bork, P. Interactive Tree Of Life (iTOL) v5: an online tool for phylogenetic tree display and annotation. *Nucleic Acids Res.* **49**, W293–W296 (2021).
70. Zhou, W. et al. Structure of the human cGAS-DNA complex reveals enhanced control of immune surveillance. *Cell* **174**, 300–311 (2018).
71. Kabsch, W. XDS. *Acta Crystallogr. D* **66**, 125–132 (2010).
72. Evans, P. R. & Murshudov, G. N. How good are my data and what is the resolution? *Acta Crystallogr. D* **69**, 1204–1214 (2013).
73. Mirdita, M. et al. ColabFold: making protein folding accessible to all. *Nat. Methods* **19**, 679–682 (2022).
74. Emsley, P. & Cowtan, K. Coot: model-building tools for molecular graphics. *Acta Crystallogr. D* **60**, 2126–2132 (2004).
75. Liebschner, D. et al. Macromolecular structure determination using X-rays, neutrons and electrons: recent developments in Phenix. *Acta Crystallogr. D* **75**, 861–877 (2019).
76. Chen, V. B. et al. MolProbity: all-atom structure validation for macromolecular crystallography. *Acta Crystallogr. D* **66**, 12–21 (2010).
77. Karplus, P. A. & Diederichs, K. Linking crystallographic model and data quality. *Science* **336**, 1030–1033 (2012).
78. Weiss, M. S. Global indicators of X-ray data quality. *J. Appl. Crystallogr.* **34**, 130–135 (2001).

Acknowledgements We thank the members of the laboratory of R.S. for comments on the manuscript and discussion; Y. Peleg and S. Albeck for assistance with protein expression; Y. Fridmann-Sirkis for help with surface plasmon resonance analysis; and H. Keren-Shaul and D. Pilzer for help with PacBio sequencing. R.S. was supported, in part, by the European Research Council (grant no. ERC-AdG GA 101018520), the Israel Science Foundation (MAPATS grant 2720/22), the Deutsche Forschungsgemeinschaft (SPP 2330, Grant 464312965), the Ernest and Bonnie Beutler Research Program of Excellence in Genomic Medicine, and the Knell Family Center for Microbiology. E.Y. is supported by the Clore Scholars Program, and, in part, by the Israeli Council for Higher Education via the Weizmann Data Science Research Center. P.J.K. was supported, in part, by the Pew Biomedical Scholars programme and The Mathers Foundation. S.J.H. is supported through a Cancer Research Institute Irvington Postdoctoral Fellowship (number CRI3996). X-ray data were collected at the Northeastern Collaborative Access Team beamlines 24-ID-C and 24-ID-E (P30 GM124165), and used a Pilatus detector (S10RR029205), an Eiger detector (S10OD021527) and the Argonne National Laboratory Advanced Photon Source (DE-AC02-06CH11357), and at beamline 8.2.1 of the Advanced Light Source, a US Department of Energy Office of Science User Facility under contract number DE-AC02-05CH11231 and supported in part by the Howard Hughes Medical Institute, the ALS-ENABLE programme and the NIGMS grant P30 GM124169-01.

Author contributions The study was conceptualized and designed by E.Y., A. Leavitt and R.S. E.Y. built and executed the computational pipeline and analysed the data. A. Leavitt

isolated the phages and conducted all of the in vivo experiments unless stated otherwise. A. Lu and P.J.K. carried out the structural analysis of Tad1 and Tad2. A.E.R. and P.J.K. determined and analysed the structure of Had1. C.A. and G.A. carried out the biochemical experiments with cell lysates and led the mechanistic characterization of the Tad2 activity. I.O. designed and conducted all of the phage knock-in experiments and the knockout of *gad2* from the phage SPβL7. J.G. designed and generated the knockdown clones. DNA cleavage experiments were carried out by S.P.A., S.E.M. and P.J.K. S.J.H. helped with the structural analysis, characterization of the Tad2 activity, and analysis of Had1 oligomerization. The study was supervised by G.A. and R.S. The manuscript was written by E.Y. and R.S. All authors contributed to editing the manuscript and support the conclusions.

Competing interests R.S. is a scientific co-founder of and adviser for BiomX and Ecophage. The other authors declare no competing interests.

Additional information

Supplementary information The online version contains supplementary material available at https://doi.org/10.1038/s41586-023-06869-w.

Correspondence and requests for materials should be addressed to Gil Amitai or Rotem Sorek.

Peer review information *Nature* thanks David Taylor and the other, anonymous, reviewer(s) for their contribution to the peer review of this work. Peer reviewer reports are available.

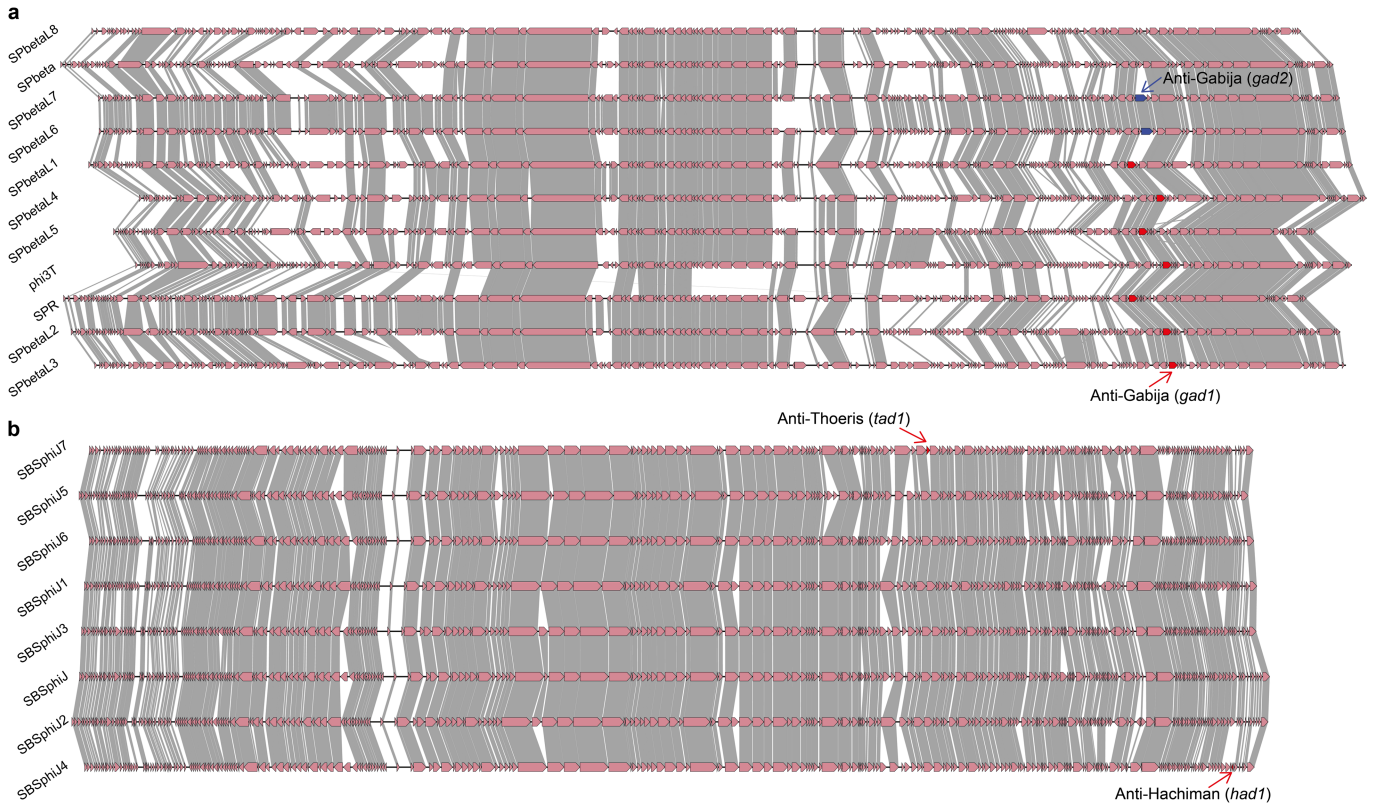

Extended Data Fig. 1 | Genome comparisons of phages from the SPbeta and SBSphiJ groups. Genome comparison of (a) eleven phages from the SPbeta group and (b) eight phages from the SBSphiJ group. Amino acid sequence similarity is marked by grey shading. Genome similarity was visualized using clinker[56].

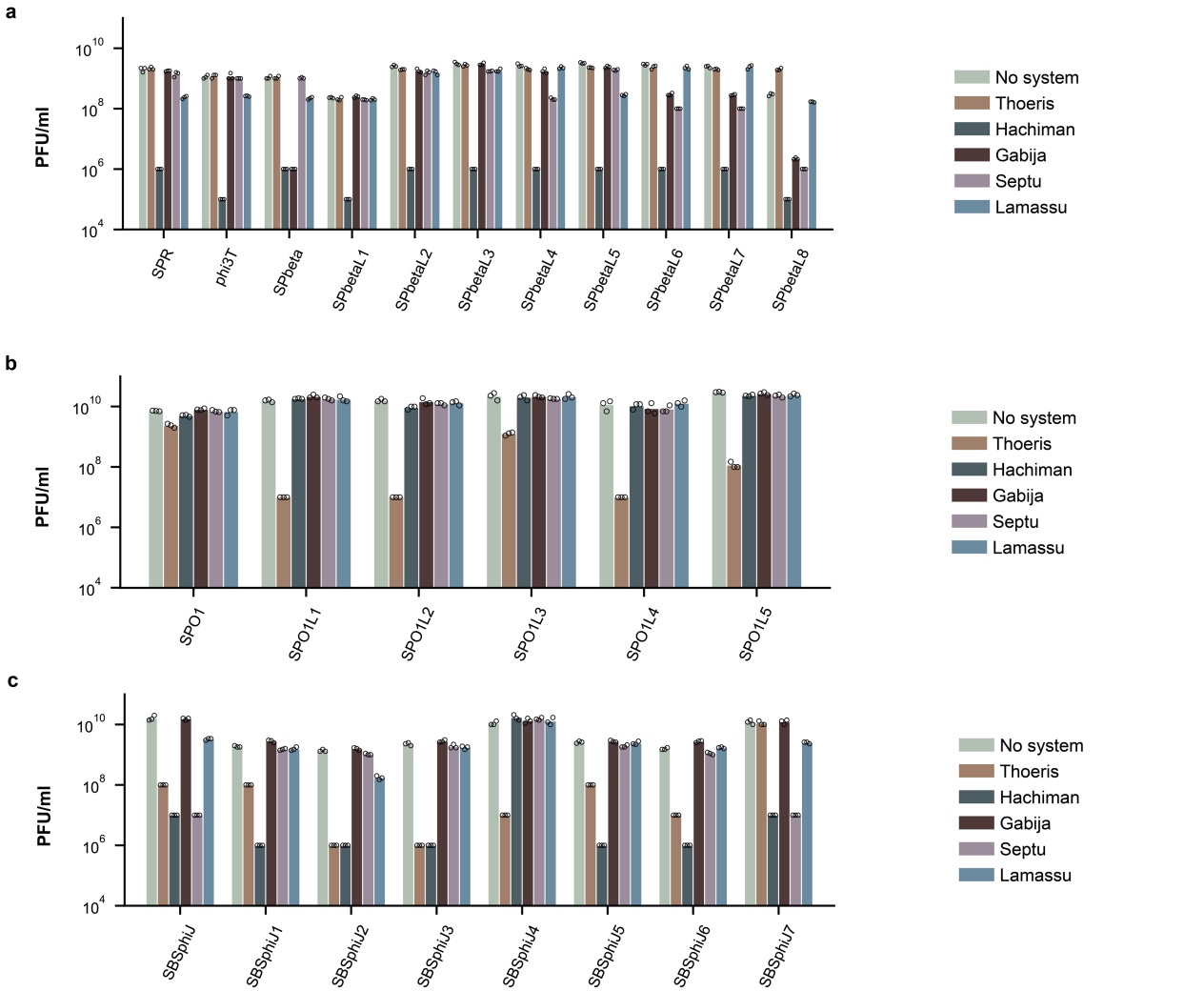

Extended Data Fig. 2 | Phages from the same family are differentially sensitive to bacterial defense systems. Results of phage infection experiments with (a) eleven phages of the SPbeta group, (b) six phages of the SPO1 group, and (c) eight phages of the SBSphiJ group. Data represent plaque-forming units per ml (PFU/ml) of phages infecting control cells ("no system"), and cells expressing the respective defense systems. Shown is the average of three technical replicates, with individual data points overlaid. The Thoeris and Hachiman data presented here are the same as those presented in Figs. 3b and 5b, respectively.

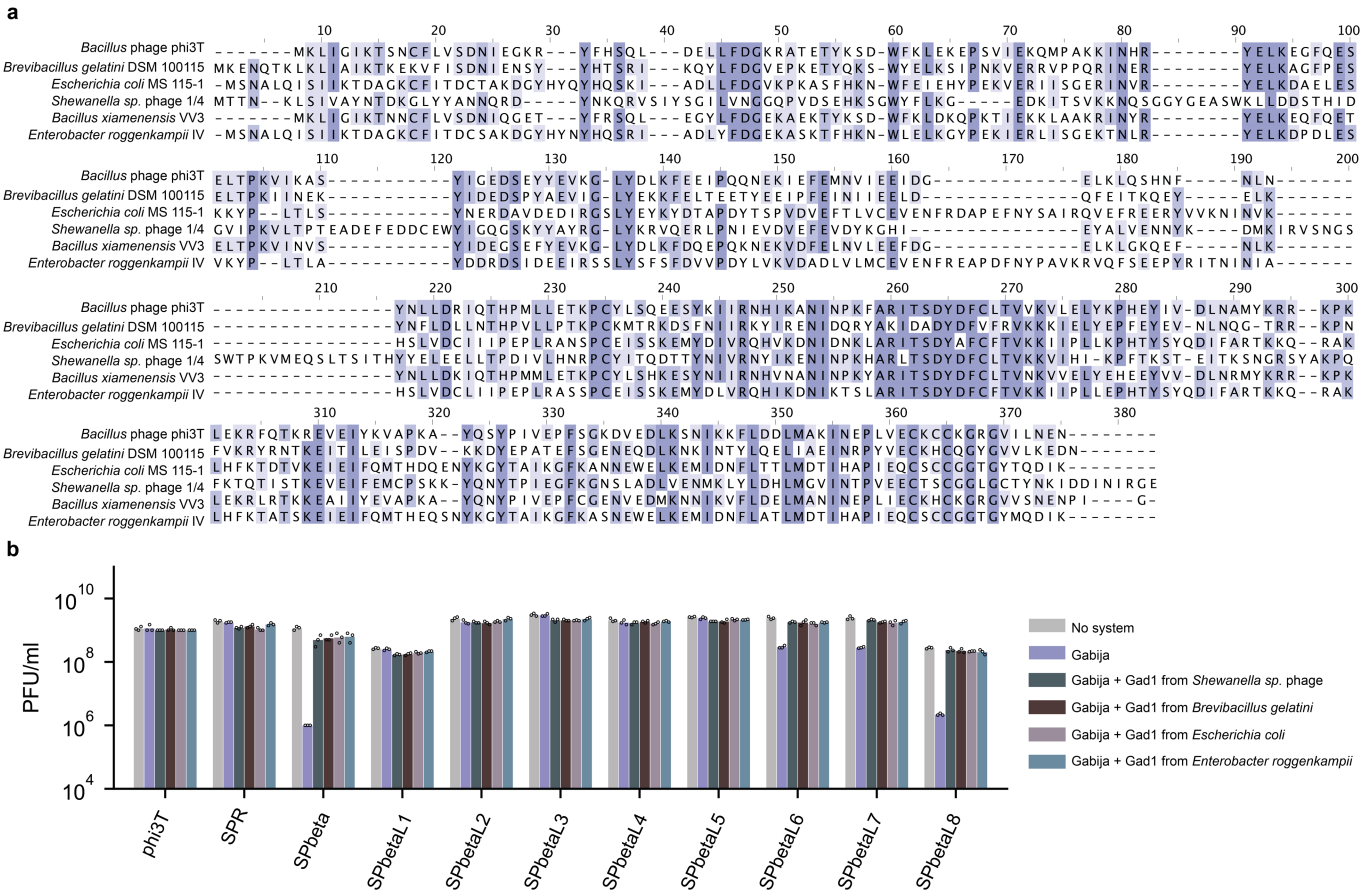

Extended Data Fig. 3 | Gad1 proteins inhibit Gabija mediated defense. (a) Multiple sequence alignment of the original Gad1 from phage phi3T and five Gad1 homologs that were chosen for experimental verification. Conserved residues are in purple. (b) Results of phage infection experiments with eleven phages of the SPbeta group. Data represent plaque-forming units per ml (PFU/ml) of phages infecting control cells ("no system"), cells expressing the Gabija system ("Gabija"), and cells co-expressing the Gabija system and a Gad1 homolog. Shown is the average of three technical replicates, with individual data points overlaid. The SPbeta data presented here are the same as those presented in Fig. 2d.

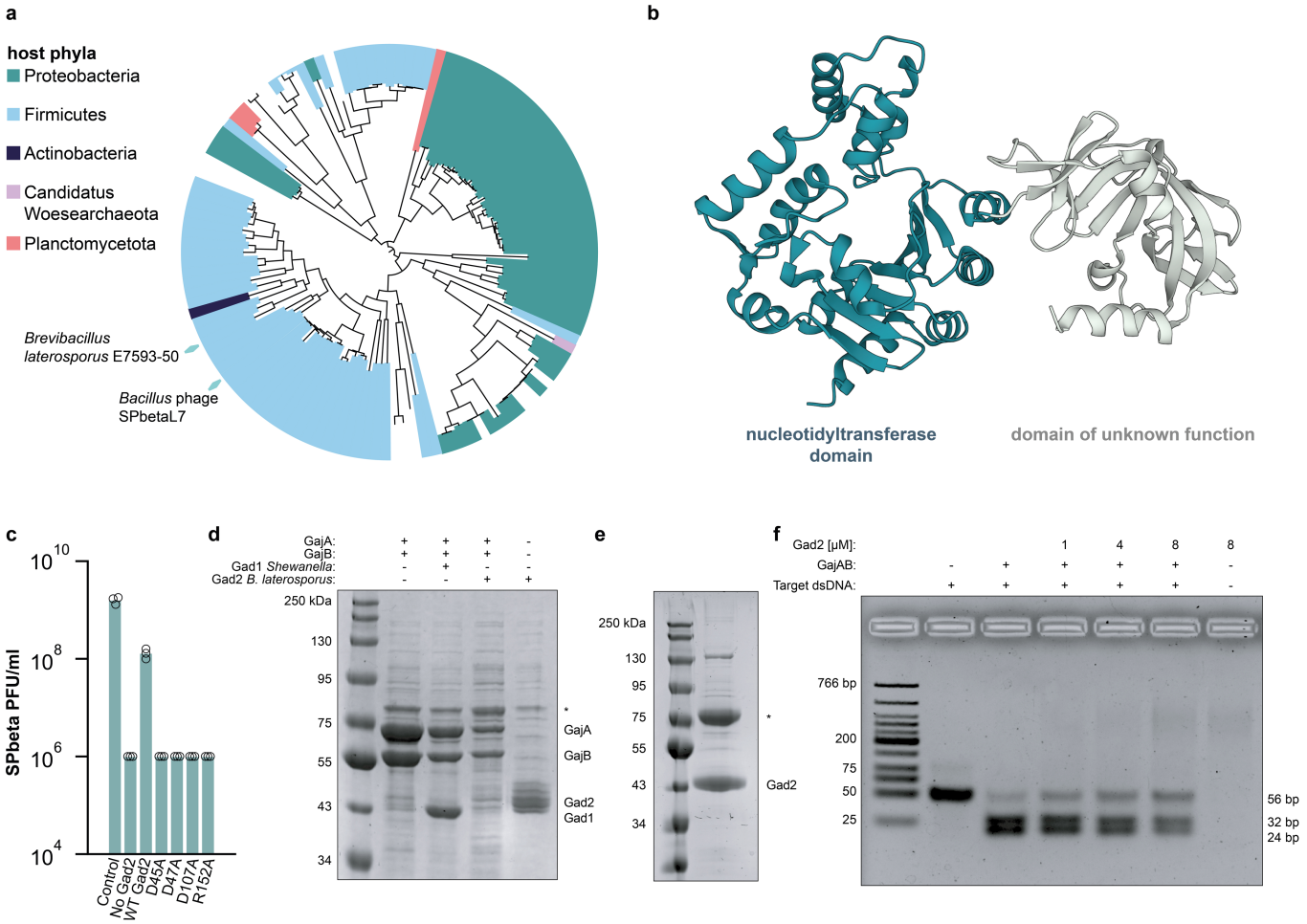

Extended Data Fig. 4 | Gad2 inhibits Gabija mediated defense. (a) Phylogeny and distribution of Gad2 homologs. Homologs that were tested experimentally are indicated on the tree by cyan diamonds. (b) An Alphafold2 model for the structure of Gad2 from phage SPbetaL7. (c) Mutations in the predicted nucleotidyltransferase active site in Gad2 result in loss of anti-defense activity. Data represent plaque-forming units per ml (PFU/ml) of phage SPbeta infecting cells co-expressing the Gabija system and WT or mutated Gad2 from *Brevibacillus laterosporus*, as well control cells expressing neither Gabija nor Gad2 ("Control") and cells expressing the Gabija system without Gad2 ("No Gad2"). Shown is the average of three technical replicates, with individual data points overlaid. (d) SDS-PAGE analysis of Ni-NTA co-purified GajAB with *Shewanella* phage 1/4 Gad1 and *Brevibacillus laterosporus* Gad2 demonstrates that Gad2 does not stably interact with the GajAB complex. Asterisk indicates minor contamination with the *E. coli* protein ArnA. Data are representative of three independent experiments. For gel source data, see Supplementary Fig. 1. (e) SDS-PAGE analysis of purified *Brevibacillus laterosporus* Gad2. Asterisk indicates contamination with the *E. coli* protein ArnA. Data are representative of three independent experiments. For gel source data, see Supplementary Fig. 1. (f) Biochemical reconstitution of GajAB DNA degradation demonstrates that Gad2 does not directly inhibit GajAB cleavage of a 56-bp target DNA. Data are representative of three independent experiments. For gel source data, see Supplementary Fig. 1.

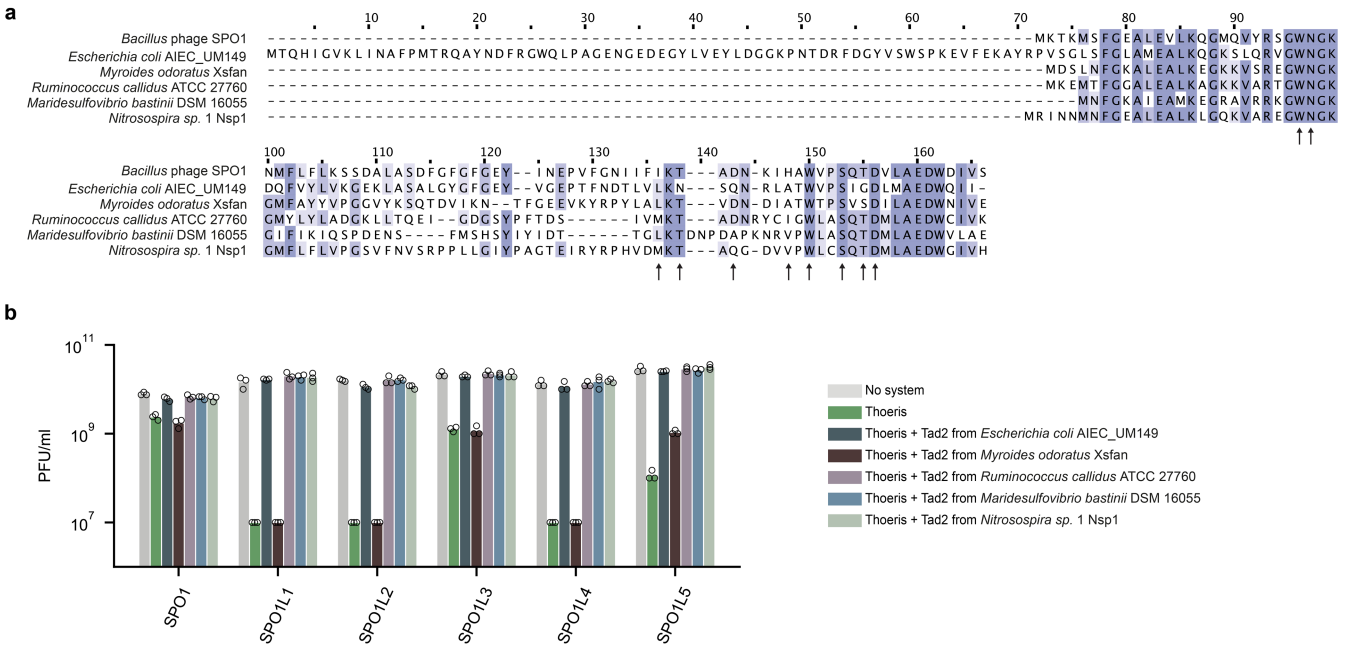

Extended Data Fig. 5 | Tad2 proteins inhibit Thoeris mediated defense. (a) Multiple sequence alignment of the original Tad2 from phage SPO1, and 5 Tad2 homologs that were chosen for experimental verification. Conserved residues are in purple. Black arrows indicate residues that are involved in 1″–3′ gcADPR binding. (b) Results of phage infection experiments with six phages of the SPO1 group. Data represent plaque-forming units per ml (PFU/ml) of phages infecting control cells ("no system"), cells expressing the Thoeris system ("Thoeris"), and cells co-expressing the Thoeris system and a Tad2 homolog. Shown is the average of three technical replicates, with individual data points overlaid.

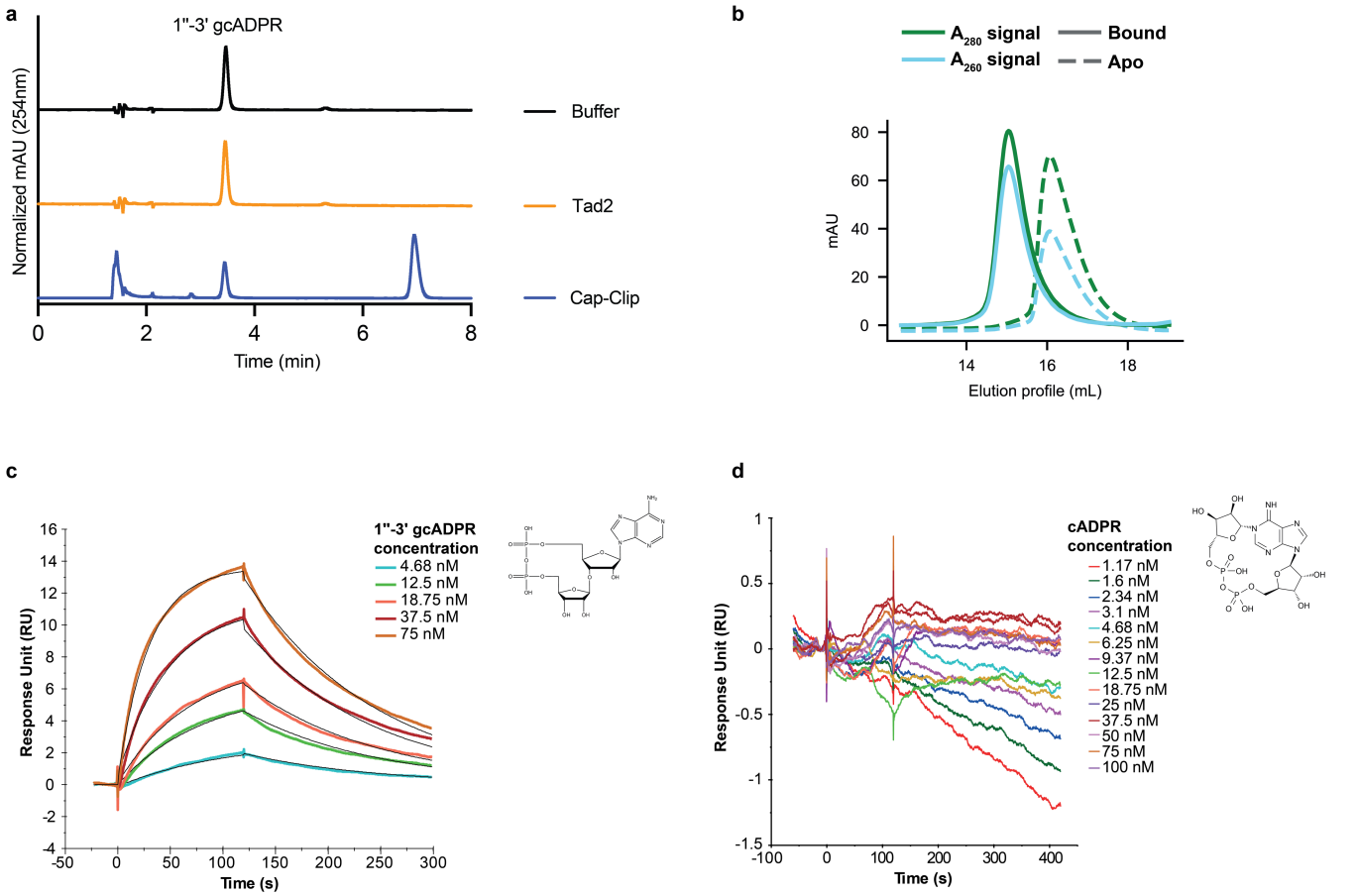

Extended Data Fig. 6 | Tad2 binds 1″–3′ gcADPR. (a) Incubation of Tad2 with 1″–3′ gcADPR in vitro does not yield observable degradation products. Representative HPLC traces of 1″–3′ gcADPR incubated with buffer, Tad2, or with the enzyme Cap-Clip known to cleave diphosphate linkages as a positive control. (b) Size-exclusion chromatography of 1″–3′ gcADPR-bound or apo state Tad2. 1″–3′ gcADPR-bound Tad2 shows a substantial shift compared to Tad2 in the apo state. (c) Surface plasmon resonance binding sensorgrams for Tad2 at five concentrations of 1″–3′ gcADPR. The black lines are the global fits using the instrument's evaluation software. ka = 3.42E + 05 ± 5.2E + 02 (1/Ms), kd = 0.00798 ± 1E-05 (1/s). (d) Surface plasmon resonance binding sensorgrams for Tad2 at multiple concentrations of cADPR.

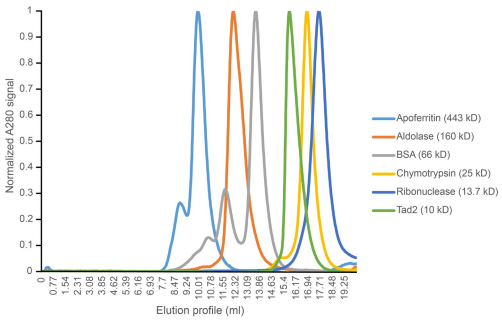

Extended Data Fig. 7 | Size-exclusion chromatography of Tad2 and various standards. Observed peak demonstrates that Tad2 forms a homomultimer.

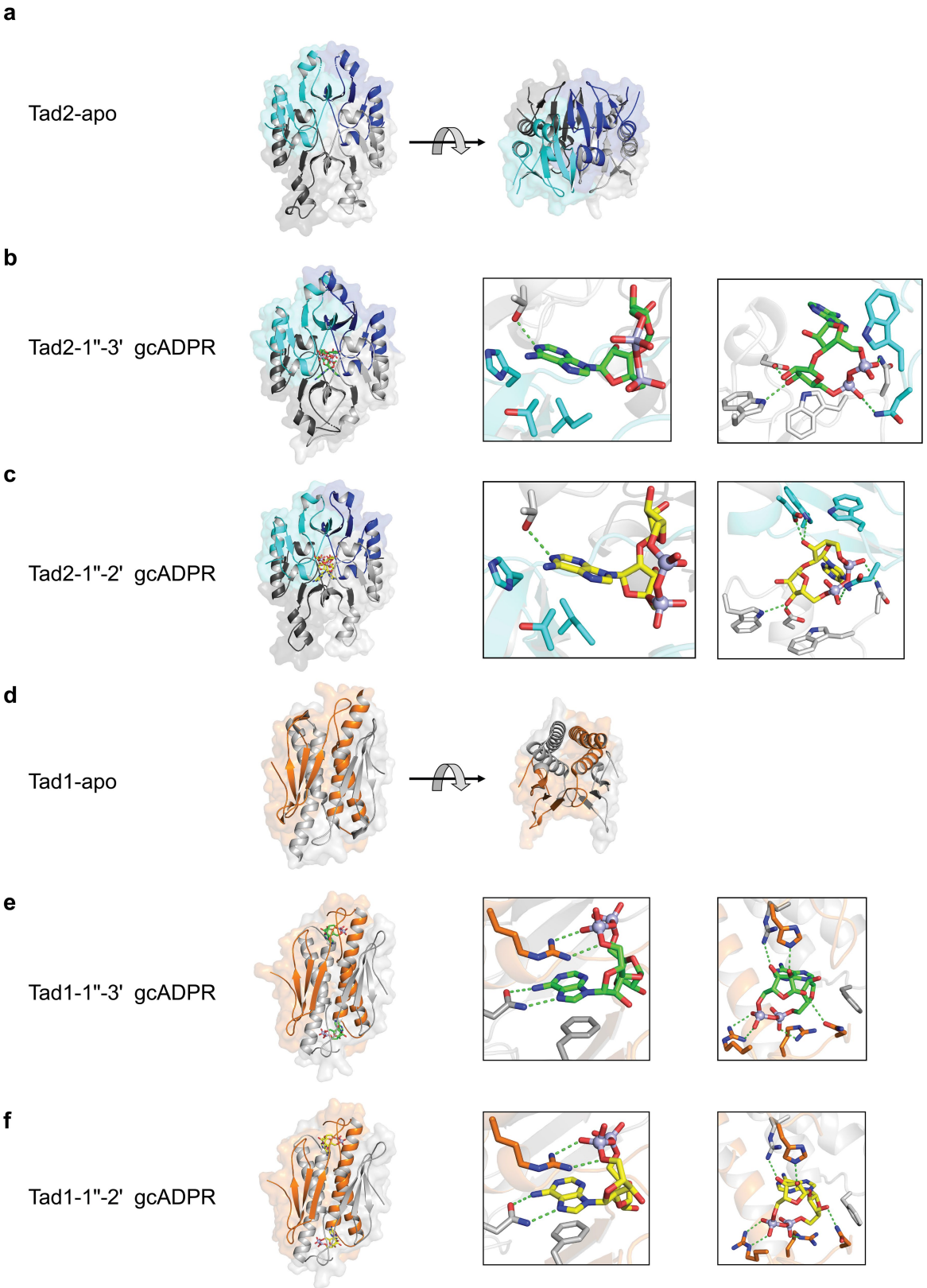

Extended Data Fig. 8 | Comparison of Tad2 and Tad1 in the apo and ligand-bound states. (a) Overview of the crystal structure of SPO1 Tad2 in the apo state in front and top view. (b,c) Overview and detailed binding pocket views of adenine interactions (left) and ribose/phosphate interactions (right) of the crystal structures of SPO1 Tad2 in complex with 1″–3′ gcADPR (**b**) or 1″–2′ gcADPR (**c**). (d) Overview of the crystal structure (PDB: 7UAV) of cbTad1 in the apo state in front view and top view. (e,f) Overview and detailed binding pocket views of adenine interactions (left) and ribose/phosphate interactions (right) of the crystal structures of cbTad1 in complex with 1″–3′ gcADPR (**e**) or 1″–2′ gcADPR (**f**, PDB: 7UAW).

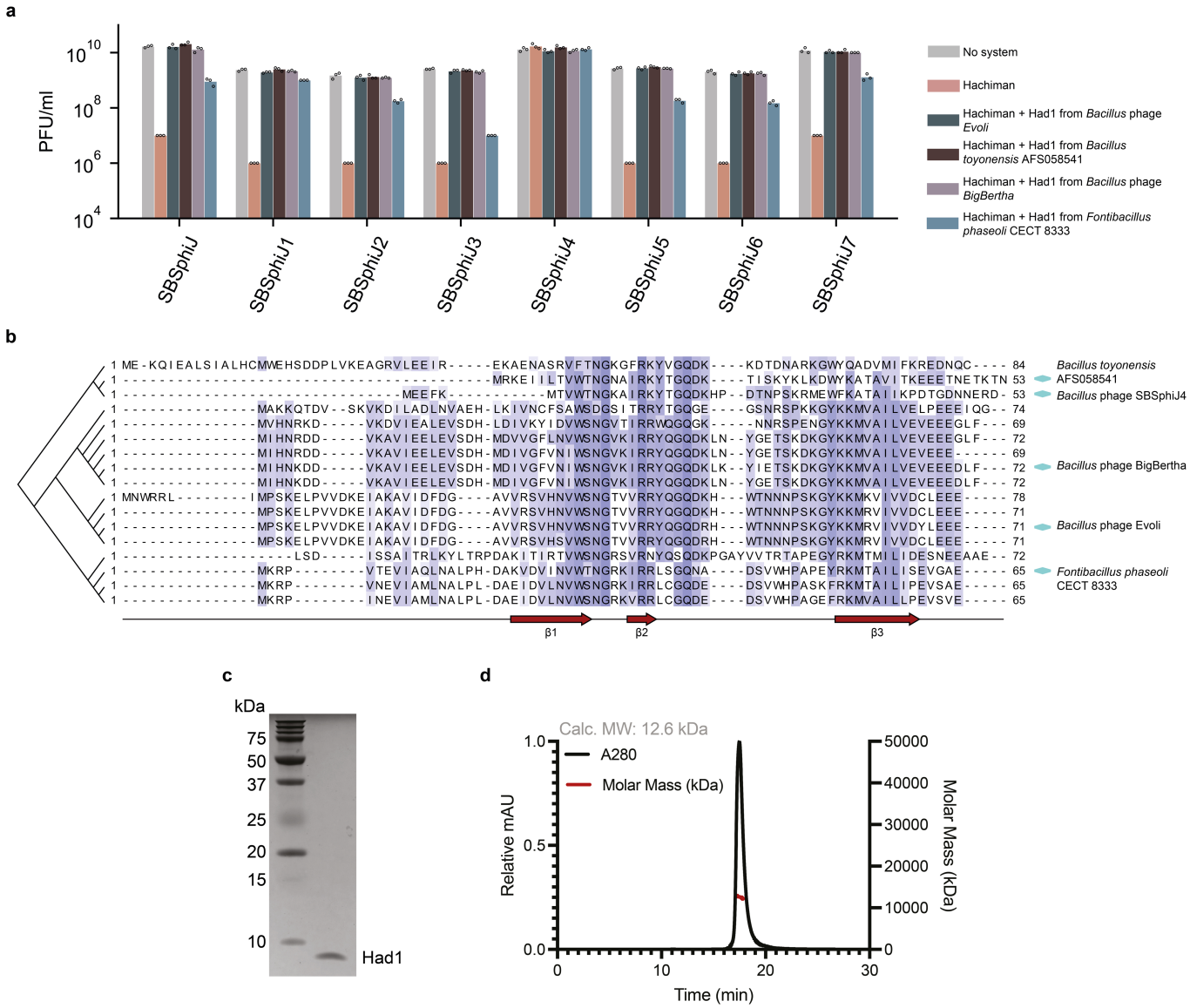

Extended Data Fig. 9 | Had1 proteins inhibit Hachiman-mediated defense. (a) Results of phage infection experiments with eight phages of the SBSphiJ group. Data represent plaque-forming units per ml (PFU/ml) of phages infecting control cells ("no system"), cells expressing the Hachiman system ("Hachiman"), and cells co-expressing the Hachiman system and a Had1 homolog. Shown is the average of three technical replicates, with individual data points overlaid. (b) Structure-guided sequence alignment of Had1 homologs colored by BLOSUM62 score. (c) SDS-PAGE and (d) SEC-MALS analysis of purified Had1. Full-length Had1 elutes as a single species that is consistent with a homodimeric complex (predicted homodimer 12.5 kDa, observed 12.6 kDa). Data are representative of three independent experiments. For gel source data, see Supplementary Fig. 1.

Extended Data Table 1 | Summary of crystallography data collection, phasing, and refinement statistics

	cbTAD1–1″–3′ gcADPR **(8SMD)**	SPO1 TAD2–apo **(8SME)**	SPO1 TAD2–1″–3′ gcADPR **(8SMF)**	SPO1 TAD2–1″–2′ gcADPR **(8SMG)**	Had1 **(8TTO)**
Data collection					
Space group	P 2_1 3	P 6_3 2 2	C 1 2 1	P 6_3 2 2	P 1
Cell dimensions					
a, *b*, *c* (Å)	95.97, 95.97, 95.97	108.40, 108.40, 74.26	94.39, 82.47, 90.76	108.06, 108.06, 72.36	30.94, 40.18, 45.29
α, β, γ (°)	90.00, 90.00, 90.00	90.00, 90.00, 120.00	90.00, 107.88, 90.00	90.00, 90.00, 120.00	75.22, 89.42, 74.91
Resolution (Å)	42.92–2.10 (2.16–2.10)	46.94–2.36 (2.45–2.36)	46.06–1.75 (1.78–1.75)	39.29–2.10 (2.16–2.10)	37.45-2.00 (2.05-2.00)
R_{pim}	2.5 (69.8)	1.9 (81.5)	5.7 (63.0)	2.2 (71.9)	0.079 (0.684)
I / σ(I)	12.2 (1.0)	19.6 (1.5)	6.5 (1.1)	17.3 (1.5)	4.9 (1.0)
Completeness (%)	99.7 (96.3)	100.0 (100.0)	98.8 (97.1)	100.0 (99.8)	97.3 (95.2)
Redundancy	13.5 (13.3)	27.0 (26.7)	5.2 (4.7)	27.5 (26.8)	1.8 (1.8)
Refinement					
Resolution (Å)	42.92–2.10	46.94–2.36	46.06–1.75	39.29–2.10	37.45-2.00
No. reflections					
Total	236478	298974	344731	414196	24521
Unique	17522	11073	65939	15065	13372
Free	876	1103	1994	1503	1327
R_{work} / R_{free}	20.12 / 23.61	26.29 / 29.87	20.77 / 24.14	22.39 / 24.99	21.53 / 25.54
No. atoms					
Protein	1984 (2 copies)	1281	5054 (8 copies)	1284 (2 copies)	1533
Ligand / ion	70	–	142	35	–
Water	60	2	599	27	172
B-factors					
Protein	61.50	86.46	24.43	72.56	31.07
Ligand / ion	55.31	–	16.62	58.93	–
Water	55.46	59.19	34.43	59.70	36.04
R.m.s. deviations					
Bond lengths (Å)	0.001	0.002	0.004	0.002	0.001
Bond angles (°)	0.433	0.434	0.795	0.463	0.41

All datasets were collected from individual crystals. Values in parentheses are for the highest resolution shell.

nature portfolio

Corresponding author(s): Gil Amitai, Rotem Sorek

Last updated by author(s): Oct 17, 2023

Reporting Summary

Nature Portfolio wishes to improve the reproducibility of the work that we publish. This form provides structure for consistency and transparency in reporting. For further information on Nature Portfolio policies, see our Editorial Policies and the Editorial Policy Checklist.

Statistics

For all statistical analyses, confirm that the following items are present in the figure legend, table legend, main text, or Methods section.

n/a	Confirmed
☐	☒ The exact sample size (*n*) for each experimental group/condition, given as a discrete number and unit of measurement
☐	☒ A statement on whether measurements were taken from distinct samples or whether the same sample was measured repeatedly
☒	☐ The statistical test(s) used AND whether they are one- or two-sided *Only common tests should be described solely by name; describe more complex techniques in the Methods section.*
☒	☐ A description of all covariates tested
☒	☐ A description of any assumptions or corrections, such as tests of normality and adjustment for multiple comparisons
☐	☒ A full description of the statistical parameters including central tendency (e.g. means) or other basic estimates (e.g. regression coefficient) AND variation (e.g. standard deviation) or associated estimates of uncertainty (e.g. confidence intervals)
☒	☐ For null hypothesis testing, the test statistic (e.g. *F*, *t*, *r*) with confidence intervals, effect sizes, degrees of freedom and *P* value noted *Give P values as exact values whenever suitable.*
☒	☐ For Bayesian analysis, information on the choice of priors and Markov chain Monte Carlo settings
☒	☐ For hierarchical and complex designs, identification of the appropriate level for tests and full reporting of outcomes
☒	☐ Estimates of effect sizes (e.g. Cohen's *d*, Pearson's *r*), indicating how they were calculated

Our web collection on statistics for biologists contains articles on many of the points above.

Software and code

Policy information about availability of computer code

Data collection	No software was used for data collection
Data analysis	Cutadapt 2.8, SPAdes 3.14.0, Prodigal 2.6.3, MMseqs2 (release 12-113e3), MAFFT 7.402, IQ-TREE 1.6.5, iTOL24 5, Phenix 1.17, Coot 0.8.9, PyMOL 2.3.0, Clinker 1.78, XDS release 2010, aimless release 2013

For manuscripts utilizing custom algorithms or software that are central to the research but not yet described in published literature, software must be made available to editors and reviewers. We strongly encourage code deposition in a community repository (e.g. GitHub). See the Nature Portfolio guidelines for submitting code & software for further information.

Data

Policy information about availability of data

All manuscripts must include a data availability statement. This statement should provide the following information, where applicable:

- Accession codes, unique identifiers, or web links for publicly available datasets
- A description of any restrictions on data availability
- For clinical datasets or third party data, please ensure that the statement adheres to our policy

Data that support the findings of this study are available within the article and its Supplementary Tables. IMG/MGV accessions, protein sequences and nucleotide sequences appear in Supplementary Tables 8–14. Coordinates and structure factors of cbTad1–1′′–3′-gcADPR, SPO1 Tad2 apo, SPO1 Tad2–1′′–3′-gcADPR, SPO1 Tad2–1′′–2′-gcADPR and Had1 have been deposited in the PDB under the accession codes 8SMD, 8SME, 8SMF, 8SMG and 8TTO respectively. The genome

sequences of phages SPO1L1-SPO1L5 and SPbetaL1-SPbetaL8 have been deposited with GenBank under accession codes OQ921336-OQ921348, respectively. Source data are available for all the main figures and for extended data figures 2,3,4,5,6,7 and 9.

Research involving human participants, their data, or biological material

Policy information about studies with human participants or human data. See also policy information about sex, gender (identity/presentation), and sexual orientation and race, ethnicity and racism.

Reporting on sex and gender	Not applicable
Reporting on race, ethnicity, or other socially relevant groupings	Not applicable
Population characteristics	Not applicable
Recruitment	Not applicable
Ethics oversight	Not applicable

Note that full information on the approval of the study protocol must also be provided in the manuscript.

Field-specific reporting

Please select the one below that is the best fit for your research. If you are not sure, read the appropriate sections before making your selection.

☒ Life sciences ☐ Behavioural & social sciences ☐ Ecological, evolutionary & environmental sciences

For a reference copy of the document with all sections, see nature.com/documents/nr-reporting-summary-flat.pdf

Life sciences study design

All studies must disclose on these points even when the disclosure is negative.

Sample size	Experiments were performed in triplicates without prior sample size calculation (unless mentioned otherwise), as is standard for such experimental designs.
Data exclusions	No data were excluded from the analyses.
Replication	Experiments were performed in triplicates. No failed replications occurred.
Randomization	X-ray crystal structures were refined using a randomly selected set of R-free reflections.
Blinding	Blinding was not required in this study as data were collected using highly quantitative measures over multiple independent replicates.

Reporting for specific materials, systems and methods

We require information from authors about some types of materials, experimental systems and methods used in many studies. Here, indicate whether each material, system or method listed is relevant to your study. If you are not sure if a list item applies to your research, read the appropriate section before selecting a response.

Materials & experimental systems

n/a	Involved in the study
☒	☐ Antibodies
☒	☐ Eukaryotic cell lines
☒	☐ Palaeontology and archaeology
☒	☐ Animals and other organisms
☒	☐ Clinical data
☒	☐ Dual use research of concern
☒	☐ Plants

Methods

n/a	Involved in the study
☒	☐ ChIP-seq
☒	☐ Flow cytometry
☒	☐ MRI-based neuroimaging

Plants

Seed stocks	Not applicable
Novel plant genotypes	Not applicable
Authentication	Not applicable